CHAPTER 1

INTRODUCTION

1.1 General

Application of stainless steel in construction industry has opened a new arena of research and increasing interest day by day throughout the world. Composite column refers to any compression member in which a steel element acts compositely with concrete element, so that both elements resist compressive force. In contrast to the encased composite column the concrete filled column offers several significant advantages over structural behavior of carbon steel structure. This is attributed to the fact that stainless steel is extremely durable, has greater corrosion resistance and improved fire resistance, and is easily maintained. Several previous projects to have utilized stainless steel include the 192 m tall St Louis, Missouri, USA (1966), the 81 m tall Parliament House Flag Pole in Canberra, Australia (1988), and the Hearst Tower at 959 Eight Avenue, New York City, USA (2006). A more recent structural use of stainless steel is in the Stone cutters bridge in Hong Kong which was completed in 2009. This bridge consists of two 298 m high towers with their upper parts comprising of a stainless-steel section filled with concrete. Due to the merits of stainless steel, it is evident that it has a very important role to play in the future design of structures, particularly when architects and structural engineers become more cognizant of the need for life cycle costing.

In the past, extensive studies have been conducted on conventional CFST columns. On the other hand, few recent studies have been carried out to investigate the behaviour of CFSST column. Most of the experimental investigations are conducted on bond behaviour, members and joints behaviour under various static loads, dynamic loads, behaviour during fire exposures and after fire exposures. Also a few numerical studies have been found on behaviour of fibre reinforced (FR) and stainless steel stiffened slender CFSST column.

CFSST columns are considered promising for their use in structural applications but research is still quite limited. Very less study has been conducted with varying different mechanical and geometric parameters as well as design code to calculate the sectional capacities of CFSST column. Also, hardly found any study on CFSST column with high strength concrete in combination with different grade of steel. The aim of this study is to conduct the experimental and numerical investigation on the behaviour of axially loaded CFSST column by varying mechanical and geometrical properties and to establish a prediction formula in compared with several existing design codes of CFST columns. This is relatively a new system for construction industry of Bangladesh. It may also contribute to enhance the BNBC on this particular subject.

1.2 Background of the Study

The composite structure is designed to enhance the benefits and performance of two elements. It provide structural steel inside the concrete or concrete inside the steel. These columns exhibit high torsional and compressive resistance about all axes when compared with the open section thereby they can reduce the size of the column in the building and increase the usable space in the floor plan. In addition, the overall column increases the general barrier of the building and offers great resistance to hunger against violent earthquakes and other years of lateral loading. Concrete-filled steel tubular (CFSST) column is a composite member which exhibit excellent composite action between stainless steel tubes and core concrete. Steel tubes provide confinement of the core concrete which significantly increase the strength and ductility of core concrete. On the other hand, core concrete delays the inward buckling of steel tube. Moreover, no form-works are needed during construction which significantly reduces the construction time and cost. Therefore, obviously the CFSST columns is going to be a very popular all over the world for the construction of mid-rise to high-rise buildings and bridges. CFSST columns exhibit higher strength, stiffness, ductility, energy dissipation and better seismic resistance compare to the reinforced concrete or steel columns

In comparison to RC, Steel and CFST Column, Concrete filled stainless-steel tubular (CFSST) columns are considered promising for their use in structural applications but research is still quite limited. Existing studies into the structural behavior of CFSST sections have generally focused on mechanical properties of stainless steel under different service conditions of stainless-steel tubes. There are differences of mechanical properties between carbon steel and stainless steel which dictates the use of CFSST Columns. Bond behaviour of CFSST columns largely differ from CFST and there are several methods to enhance the bond strength in particular regions.

Failure modes and load versus deformation curves of CFSST columns with various cross-section types under different loading conditions are stated in comparison with conventional concrete filled steel tubular (CFST) columns manufactured with carbon steel. Cyclic tests on CFSST columns show that the columns have high strength and ductility and good energy-dissipation capacity, justifying the use in seismic-prone areas. Meanwhile, impact tests on CFSST columns demonstrate that they can be used as piers in bridges or as exterior columns in buildings. Behaviour of CFSST columns in fire and after fire exposure is worth discussing due to the superior performance of stainless steel at elevated temperatures. Composite joints, including hybrid beam-column joints, T-joints and X-joints, are commonly used in engineering practice.

However, in the context of concrete-filled elliptical hollow members, only limited previous experimental and numerical studies have been carried out, design rules for CFSST members are not yet available. Therefore, this research aims to is to conduct investigation on the behaviour of axially loaded CFSST column on the basis of fundamental theory, experimental analysis, numerical simulations and statistical verification. The proposed design rules are suitable for incorporation into structural design codes. This is relatively a new system for construction industry of Bangladesh. It may also contribute to enhance the BNBC on this particular subject.

1.3 Objectives and Scope of the Study

The objectives of this research are as follows:

a) To investigate CFSST stub columns experimentally under axial load.

b) To develop a nonlinear 3D finite element model of CFSST.

c) To determine the influence of mechanical and geometric properties on the behaviour and strength of CFSST columns.

d) To propose a prediction formula for sectional capacity of CFSST column based on existing design codes of conventional CFST column.

It is expected that this study will provide a thorough understanding of the behavior of CFSST columns. Limited research works have been carried out in the past, no such study has been performed until date, which has focused on both conventional and high-strength CFSST stub and long columns under concentric and eccentric loading condition. It will also give an idea about the conservatism of the current design standards for predicting the ultimate capacity of CFSST columns.

The experimental investigation into the structural behavior as well as numerical models of CFSST columns have been developed using FE software ABAQUS 6.14, considering geometric and material nonlinearity. The developed finite element models will be further validated against the current experimental investigations done in laboratory as well as investigation result of recently published renowned papers. Current experimental results and recently published experimental results showing the capability of numerical models to accurately predict the experimental results. Once the FE models are validated, extensive parametric study was conducted to generate additional results for a wide range of parameters.

All the columns used in the parametric study have a constant cross-sectional dimension of 450 mm × 450 mm (B mm × D mm), representing a fairly large size composite column for a typical high-rise structure. These columns are designed and analyzed during the parametric study to incorporate the effects of several geometric and material parameters that can significantly affect CFSST column behaviour. The variables are the load eccentricity ratio (e/D), depth-to-thickness ratio (D/t), column slenderness ratio (L/D), concrete compressive strength (f'c), and 0.2% proof strength ($\sigma_{0.2}$) of stainless steel. The effects of those parameters on the compressive behavior of CFSST columns will be studied to investigate the load-deformation response, ultimate compressive capacity, failure mode, axial load versus lateral deflection response, moment versus lateral deflection response, and axial load-moment interaction diagram of CFSST columns. Finally, a comparison will be presented between the numerical results and the predicted capacities using AISC-LRFD 2010 design equations. The limitation of this study is shrinkage of concrete is not considered in the experimental study, as well as only square section is used for axially concentric load.

1.4 Organization of the Thesis

This thesis is divided into six chapters. An introduction to the study is presented in

Chapter 1. It includes the research background, objectives and the scope of the study.

Chapter 2. Presents a brief review on the literature related to CFSST columns and explores in relative detail the experimental and analytical research works carried out on CFSST columns.

Chapters 3. Focus on experimental investigations into the structural behavior of CFSST columns. A comprehensive experimental program including material tests and full-scale member tests has been presented along with subsequent analysis based on the experimental results.

Chapter 4. The detailed description of the finite element model for CFSST columns, along with the properties of the test specimens from published literature. The selected element types, mesh configuration, material mechanical properties for steel and concrete and the solution strategy implemented in the finite element model were also presented.

Chapter 5. This chapter includes the comparison between the experimental and numerical analysis, failure modes, peak axial loads, axial strains at peak load, load versus axial deformation curves for different test groups.

Chapter 6. Presents the detailed parametric study conducted with the developed finite element model to cover the range of several geometric and material parameters on the behaviour of CFSST columns. The findings of this parametric study are demonstrated and discussed in detail.

A summary of the methodology and conclusions regarding the achievements of this research works are included in Chapter 7, along with the recommendations for future research.

CHAPTER 2

LITERATURE REVIEW

2.1 Introduction

This chapter contains an overview of previous research on the stainless-steel hollow and concrete filled columns and columns with different shapes. It covers research results on experiments, digital simulations and simplified design methods.

Composite columns are mainly made of combining steel and concrete in order to beneficially utilize the desired property of both the material. They are typically classified in three groups: concrete filled tubes (CFT), fully encased composite (FEC) columns and partially encased composite (PEC) columns. Concrete filled steel tube is a composite structural member consist of steel tube and concrete core inside which having many advantages, first: the concrete core can prevent the inward buckling of steel box. Second, the confinement provided by the steel box can enhance the mechanical properties of the concrete. Third, the concrete infill is confined by steel tube increasing the strength and ductility of the concrete core in steel tube. Finally, no formwork and reinforcement are required to cast the concrete. As a result, these columns provide extra strength and stiffness in an economical and environmentally friendly manner. CFT has various cross-sections like circular, square, rectangular and multi-side. Among these circular, rectangular and square sections are widely used in construction works.

Until the 1950s, it was normal practice to use a wet mix of low strength concrete in CFT to neglect the contribution of the concrete in the strength of the column. Tests by Faber (1956), Stevens (1959) and others then showed that savings could be made by using better quality concrete and designing the column as a composite member. This empirical method was developed by stages from earlier design procedures for steel columns, and is not based on fundamental research on composite columns. In the mid-1980s several buildings constructed at Seattle in USA became well known for their use of concrete filled steel tubes. Many developed countries like USA, Japan, Germany, Singapore, Australia, Canada, Belgium etc., adopt this kind of composite sections to facilitate speedy construction. Because of the increased use of composite columns, many experimental and theoretical research works have been carried out to study the strength and behaviour of the CFT columns. Rational methods of designing CFT columns have also been developed.

Initially, American Concrete Institute (ACI) and American Institute of Steel Construction (AISC) provided rules for the design of these structural elements. In the United States of America a joint Structural Specifications Liaison Committee (SSLC) was organized in 1978 to evaluate the acceptability of composite column design procedure. The numbers of versions on AISC-LRFD specifications and ACI-318 were issued in different time successively. Other specifications or codes that provided the rules for design of composite structure were the Euro code (ENV 1994), the Building Code of Australia (BCA, 2005), the Architectural Institute of Japan (AIJ, 1997), and the New Zealand building code (the NZBC1992) standards. However, ACI-318, AISC-LRFD, and Euro code 4 are being widely used around the world for the design of composite structure. Recently Bangladesh National Building Code (BNBC-2015) has incorporated steel-concrete composite structure in chapter-13.

In the last few decades, the application of stainless steel in construction has attracted increasing interests among researchers and structural engineers. Compared with conventional carbon steel, stainless steel has several advantages, such as extremely high durability and corrosion resistance, easiness of maintenance and improved fire resistance. However, the high cost of stainless steel prevents its wide application as a structural material. To make more economical use of stainless steel, it is advisable to develop stainless steel-concrete composite structures. A good example is to fill stainless steel hollow sections with concrete to form concrete filled stainless steel tubes (CFSST). Figure 2.1 shows typical cross-sections of circular and square CFSST columns, where D is the diameter of the circular steel tube, and B is the width of the square steel tube.

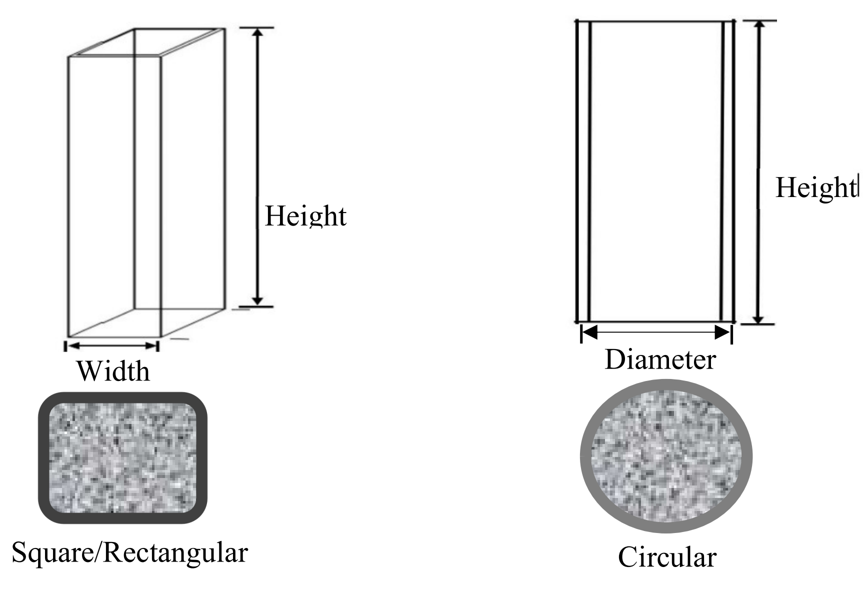

Figure. 2.1 Typical cross-sections of circular and square CFSST columns.

In the past, extensive studies have been conducted on conventional concrete filled carbon steel columns and their behaviour has been well understood. Since the material behaviour of stainless steel is different from that of conventional carbon steel, some recent studies have been carried out to investigate the behaviour of CFSST members and joints. This is necessary to allow the development of rational design guidelines for this type of innovative composite structure. In recent past number of experimental and numerical investigations has been conducted on the bond behaviour of CFSST, members and joints under various loading conditions, including static loading, dynamic loading, as well as joints under static loading and fire.

2.2 Types of Composite Columns

Fully encased composite (FEC) columns Figure 2-2(a) to 2-2(c) are columns consist of structural steel sections encased by concrete where the structural steel area comprises of at least four percent of the total composite column cross sections. A partially encased composite (PEC) Figure 2-2 (d) to 2-2 (e) column is a type of composite column that generally consists of an H-shaped steel section with concrete cast between the flanges. One of the advantages of this type of column over fully encased columns is that it requires formwork on only two sides of the column. In the mid-1990s, the Canam Group Inc. (Canam) developed a new design for PEC columns intended to make it more economical, particularly for mid- and high-rise steel structures. A Concrete filled tube (CFT) Figure 2-2 (f) to 2-2 (i) column is a structural system with excellent structural characteristics, which is the result of combining the advantages of a tube and those of concrete. A CFSST column is constructed by filling a hollow rectangular or circular structural stainless steel tube with concrete. As a structural system, a CFSST column has a high load bearing capacity, excellent earthquake-resistance, good ductility, corrosion resistant and its higher stiffness which delays the onset of local buckling. Besides that, the stainless steel tube can function as a permanent formwork as well as reinforcement, thus more economical to be utilized. The structural properties of the CFSST columns increase due to the composite action between the constituent elements. The steel tube acts as longitudinal and transverse reinforcement. The steel tube provides confining pressure to the concrete so a tri-axial state of stress is created.

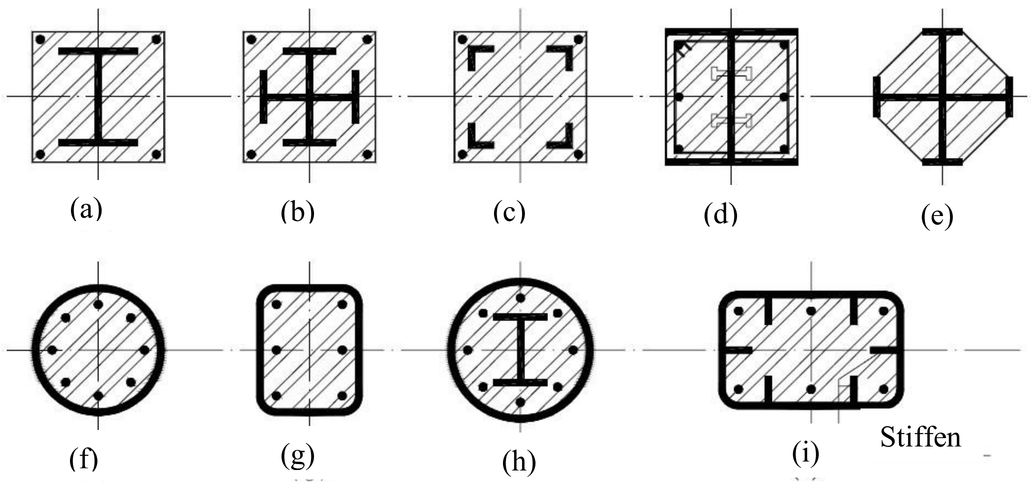

Figure 2.2: Detail X-sections of different composite columns, (i) FEC columns (a)-(c); (ii) PEC columns (d)-(e); (iii) CFSST columns (f)-(i). (Source:Post graduate dissertations (Thesis) of Department of Civil Engineering (CE), BUET.

2.3 Research on Concrete Filled Steel Tubular Column.

CFSST is very new in the construction industry and researches on this field also very less in comparison to the conventional steel structure. Based on the previous research a few of the are reviewed in subsequent paragraphs.

2.3.1 Bond Behaviour of Concrete Filled Tubes

Bond between the tube and core concrete could play a key role in the composite action between the two components. Sufficient bond strength is necessary to ensure the possible shear force transfer in a composite column. However, compared with the inner surface of a carbon steel tube, that of the stainless-steel tube is generally smoother since it can be free of rust. This may lead to a reduction in the bond strength in stainless steel composite columns. In order to evaluate the influence of using stainless steel on the bond strength, there are few studies carried out by Z. Tao et al. (2016); Y. Chen et al. (2017) and T. Y. Song et al. (2017). Findings of these experimental investigations are presented below:

Tao et al. (2016) carried out push-out tests, where the main parameters were the cross-sectional dimension (120–600 mm), steel type (carbon and stainless steels), concrete type (normal, recycled aggregate and expansive concretes), concrete age (31–1176 days), and interface type (normal interface, interface with shear studs and interface with an internal ring).

Before filling concrete, values of the average surface roughness (Ra) were measured for typical steel tubes. The typical surface conditions of stainless steel and carbon steel tubes are shown in Fig. 2.3. It was found that average surface roughness (Ra) of stainless steel could vary significantly among different products. The internal surface finish of the stainless steel tube in specimen SS200N1 represents typical 2B surface finish, whilst the internal surfaces of the tubes in specimens SC200N1 and SC600N1 are typical carbon steel surfaces with no or light rust. It was found that the Ra value of a stainless-steel tube was only about a half of that of the carbon steel counter part. For this reason, the measured bond strengths between the stainless-steel tube and concrete in CFSST columns decreased by 32% to 69% compared with the bond strengths in conventional CFST columns as shown in Fig.2.4.

For some regions in structures, the demands for bond may be very strong, such as connections, foundation supports, and braced frames. Therefore, the bond strength reduction in CFSST columns may need to be considered when there is a need of potential load transfer between the stainless steel tube and concrete. To enhance the bond strength, several approaches have been proposed, such as welding internal ring (s) on to the inner surface of the steel tube, welding shear studs and using expansive concrete. Welding internal rings is the most effective method, followed by welding shear studs and adopting expansive concrete. However, further research is required to develop design guidelines to facilitate the use of these methods. Chen et al. conducted a series of repeated push-out tests on CFSST columns for bond-slip behaviour of concrete-filled stainless steel circular hollow section. It was confirmed that about 70% of the bond strength in a CFSST column is from the interface friction force, whilst the remaining 30% of the bond strength is contributed by the chemical adhesive force and the mechanical interlock force.

Chen et al. (2017) conducted a series of repeated push-out tests on CFSST columns. It was confirmed that about 70% of the bond strength in a CFSST column is from the inter-face friction force, whilst the remaining 30% of the bond strength is contributed by the chemical adhesive force and the mechanical interlock force.

Song et al. (2017) carried out further tests to investigate the post-fire bond behaviour of CFSST columns, where the specimens were heated in the furnace to a target temperature of 800 °C before conducting the push-out test. They found that the bond strength of CFSST specimens was generally lower than that of the CFST specimens after fire. However, when the concrete age was relatively long (over six months), the influence of steel type on the bond strength was reduced due to the influence of concrete shrinkage.

Ra =5.97μm (CS 400N1, stainless steel)

Ra = 2.61μm (SS 200N1, Stainless steel)

Ra=9.88μm (CC400N1, Carbon steel)

Ra=4.77μm (SC200N1, Carbon steel)

Ra= 4.35 μm (SC600N1, Carbon steel)

Figure. 2.3 Surface roughness of stainless steel and carbon steel (Source: L-H. Han et al/ Journal of Constructional Steel Research)

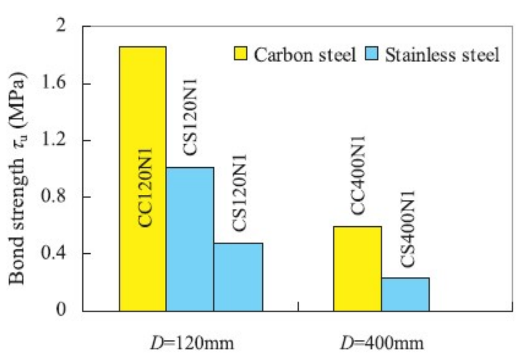

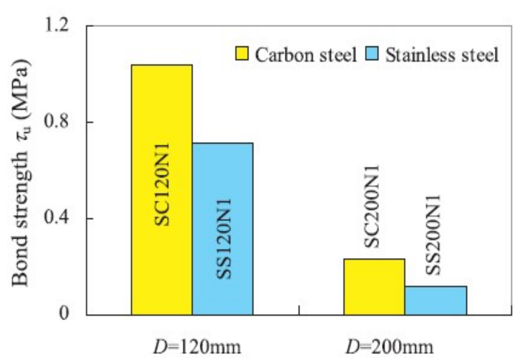

Figure. 2.4 Bond strength of stainless steel and carbon steel (Source: L-H. Han et al/ Journal of Constructional Steel Research)

2.3.2 Confinement Effect of CFSST Columns

Confined concrete structural member especially compressive member are defiantly performed better than the unconfined members. The behavior of the columns due to the confinement was investigated by Dabon, Khoriby, El-Boghdadi and Hussanein discuss as below:

Dabaon, Khoriby, El-Boghdadi and Hassanein (2009) has worked on Confinement effect of stiffened and un-stiffened concrete-filled stainless-steel tubular stub columns. There a comparative study is done between stiffened and un-stiffened concrete-filled stainless steel hollow tubular stub columns using the austenitic stainless-steel grade EN 1.4301 (304). Finite element analysis of concrete-filled stainless steel un-stiffened tubular stub columns is constructed herein based on the confined concrete model. It is then compared with the experimental results of concrete-filled stainless steel stiffened tubular stub columns. The stiffened stainless-steel tubular sections were fabricated by welding four lipped angles or two lipped channels at the lips. The longitudinal stiffener of the column plate was formed to avoid shrinkage of the concrete and to act as a continuous connector between the concrete core and the stainless-steel tube. The behavior of the columns was investigated using two different nominal concrete cubic strengths of 30 MPa and 60 MPa. The overall depth-to width ratios (aspect ratio) varied from 1.0 to 1.8. The depth-to-plate thickness ratio of the tube sections varied from 60 to 90. The stiffened and un-stiffened concrete-filled stainless steel tube specimens were subjected to uniform axial compression over the concrete and stainless steel tube to force the entire section to undergo the same deformations by blocking action. The results of the comparative study showed that the stainless steel tubes in stiffened concrete-filled columns offered a high average of increase in the confinement of the concrete core than that of the un-stiffened concrete-filled columns. The results of the comparative study showed that the stiffened concrete-filled columns offered an average of 43% increase in the column strength over that of the un-stiffened concrete-filled columns. However, this increase in the overall strength of the stiffened concrete-filled columns is accompanied by a relatively small increase in the cross-sectional area of the stainless steel tube. Also, the comparative study showed that the stainless steel tubes in stiffened concrete-filled columns offered an average of 33% increase in the confinement of the concrete core over that of the un-stiffened concrete-filled columns (taking into account the effect of initial imperfection and welding residual stresses in the stiffened stainless steel tubes). Author found that the design rules specified in the ASCE Standard are generally conservative for un-stiffened concrete-filled stainless steel square and rectangular stub columns, while they are highly conservative for stiffened concrete-filled stainless steel square and rectangular stub columns.

2.3.3 Experimental Investigations

Experimental investigation is the most effective way to carry out research works. In the past, extensive studies have been conducted on conventional concrete filled carbon steel column and their behavior but limited experimental studies have been conducted CFSST columns. Experimental researches were carried out on CFSST by several research groups (Brain Uy, Zhong Tao and Lin-Hai Han, 2011; Lu YQ & Kennedy DJL, 1994; M.A. Dabaon, M.H. El-Boghdadi, M.F. Hassanein, 2009; Young and Lui (2005): Ghannam et al. (2011): D. lam, L.Gardner, M. Burdett, 2010) to investigate the behaviour of columns under various loading conditions. Findings of these experimental investigations are presented below:

Lu YQ & Kennedy DJL (1994), conducted experimental research on the evaluation of the flexural force and stiffness of the CFSST column filled with normal weight concrete. Virdi PJ & Dowling KS achieves the strength of bonding between concrete and steel in the CFSST column by providing different mechanisms for bonding without shear links. Shaker Khalil investigated the relationship between steel and concrete in the CFSST column by assessing the ratio of load versus tape with pressure test. Research on CFSST columns with additional steel reinforcements was also conducted to improve their behavior.

M.A. Dabaon, M.H. El-Boghdadi, M.F. Hassanein (2009), conducted experimental investigation on concrete-filled normal strength stiffened stainless steel stub columns using the austenitic stainless steel grade EN 1.4302 (304). A test program of concrete filled normal strength, five concentrically loaded slender stiffened columns and ten concrete stiffened columns have been presented. The columns in this investigation were stiffened by two methods; using longitudinal stiffener in addition to infilled concrete, main variable was stainless steel tube and in-filled concrete strength. It was observed that the column strength of the concrete-filled stainless steel stiffened tubular stub columns was considerably higher than that of the stiffened slender stainless steel hollow tubular stub columns. The average values of the column strength of columns in-filled with a concrete of 34.8 MPa mean compressive strength divided by that of the stiffened slender stainless steel hollow tubular stub columns is equal to 3.63. This ratio was about 4.48 in case of the columns in-filled by a concrete of 61.9 MPa mean compressive strength. However, different failure modes were observed from the test series. The mode of failure of the stiffened slender stainless steel hollow tubular stub columns was due to local buckling. Once local buckling has occurred, in concrete-filled stainless steel stiffened tubular stub columns, by the time of reaching the test strength, the stainless steel tube was not able to provide confinement for the concrete. The column capacity, at this stage, was governed by local buckling failure mode. Another observation that can be noticed from the experimental tests is that the stiffeners contributed largely to the test strength. P_{test} of columns even when the stiffeners' rigidities were small, because the local buckling of longitudinal stiffeners was prevented by the concrete.

The column strengths of the stiffened square concrete-filled columns of concrete strength C60 and C30 were increased by 156% and 105% over that of the stiffened hollow-section column due to the existence of concrete. The increase in the column strength was 259% and 239% for the stiffened rectangular concrete-filled columns of concrete strength C60 and C30 over the Rectangular hollow section. It could be seen that the in-filled stiffened column had a considerably higher stiffness than that of the stiffened hollow-section column resulting in a sharper load_axial shortening behaviour.

Young and Lui (2005) presented the behavior of cold-formed high strength stainless steel sections. Their test specimens were cold-rolled from flat strips of duplex and high strength austenitic stainless steel. The material properties of high strength stainless steel square and rectangular hollow sections were determined. Tensile coupons at different locations in cross section were tested. Hence, the distributions of 0.2% proof stress and tensile strength measured in the cross section of cold-formed high strength stainless steel sections were plotted. The material properties of the complete cross section in the cold-worked state were also obtained from stub column tests. Detailed measurements of initial local geometric imperfections of the sections were obtained. The initial local plate imperfection profiles were plotted. Residual stress measurements of the high strength stainless steel sections were also conducted. The membrane and bending residual stress distributions in the cross section of the specimens were obtained. Furthermore, authors compared the stub column test strengths with the design strengths.

Ghannam et al. (2011) tested twelve (12) experimental samples under concentric loading. The columns were lightweight and used ordinary concrete to fill steel pipe columns. The shape of the columns was circular and square. Concrete strengths were 10 MPa and 33.4 MPa. The tensile strength in the steel sectors was 320 MPa, 360 MPa in the rectangle, 350 MPa and 355 MPa for circular columns. The columns were of different sizes, shapes, lengths and proportions. The purpose of the research was to verify the behavior and comparison of the normal and light concrete pipe under axial loading.

Different codes are available for evaluating the strength of concrete filled tube. American Institute of Steel Construction (AISC) and the American Concrete Institute (ACI) provided rules for the design of these structural elements. In the United States of America a joint Structural Specifications Liaison Committee (SSLC) was organized in 1978 to evaluate the acceptability of composite column design procedure. Successively, the numbers of versions on AISC-LRFD specifications and ACI-318 were issued in different time. Other specifications or codes that provided the rules for design of composite structure were the Euro code (ENV 1994), the Architectural Institute of Japan (AIJ, 1997), the Building Code of Australia (BCA, 2005). Among all the codes ACI-318, AISC-LRFD, and Euro code 4 are used all over the world. Before describing the experimental, numerical and codes comparison a short note about composite columns are discussed in subsequent.

B. Uy et al, (2011) carried out an experimental study by including 60 short CFSST columns under axial compression or combined actions of compression and bending, 24 CFSST slender columns and 33 reference short empty stainless steel hollow sections. The test results revealed that the failure modes of CFSST columns are generally similar to those of conventional carbon steel CFST columns. However, due to the increased ductility, the stainless steel composite columns showed far higher capacity of axial deformation and larger amplitudes of local outward bulges. The schematic failure modes of hollow steel tubes, CFST and CFSST are presented in Figure. 2.5 and Figure 2.6 illustrates the typical measured axial load versus axial strain (N - ε) curves of the CFSST stub columns, where the axial load is normalized with respect to the maximum load Nmax. Generally, the N- ε responses could be classified into three types, which depend mainly on the confinement of the stainless steel tube to concrete. If the confinement was strong enough, the N - ε relationship showed a strain hardening response (Type A) with continuous strength increase from Point 1 to Point 2. As less confinement was provided, Type B curve had a strain softening portion 1′2′ after reaching the first peak Point 1′. Because of the strong strain-hardening effect of stainless steel, the load increased once again to Point 3′ at the end of the test. Type C is the typical N–ε relationship with a strain-softening response which is very common for conventional carbon steel CFST stub columns. Generally, the residual strength of the “Type C” CFSST stub column was much higher than that of a carbon steel composite counterpart. It is evident that the stainless steel tube could provide better confinement for its core concrete at the late loading stage compared with the carbon steel tube in a CFST column.

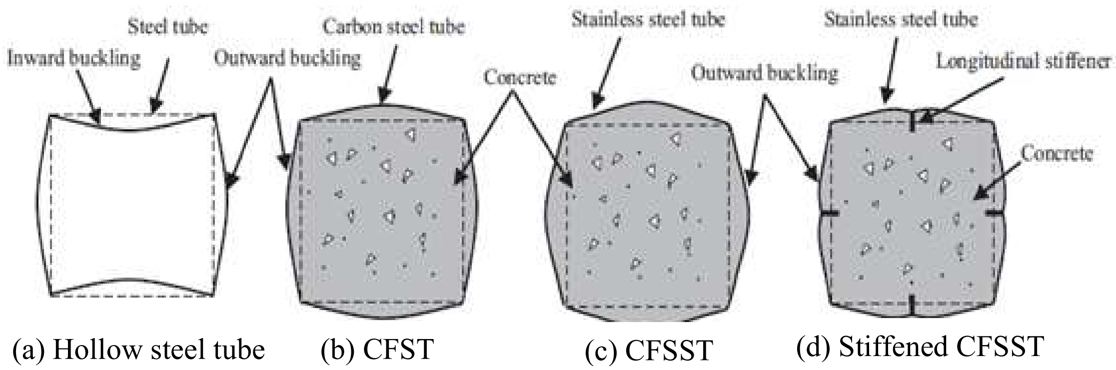

Figure. 2.5 Schematic failure modes of stub columns (Source: L-H. Han et al/ Journal of Constructional Steel Research).

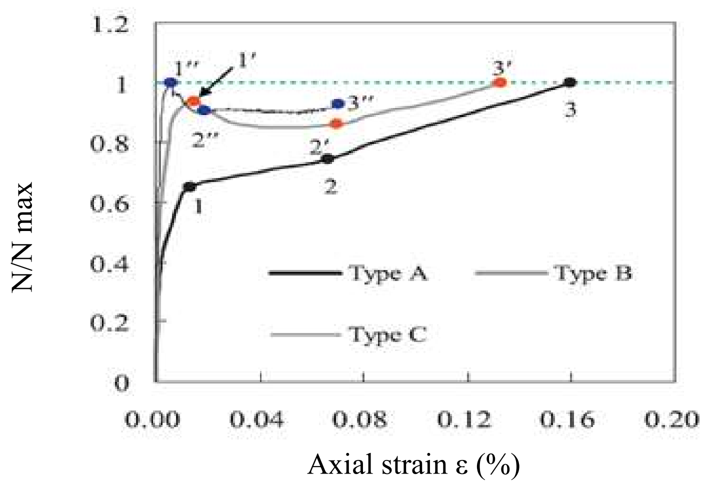

Figure. 2.6 Typical axial load versus axial strain of CFSST columns (Source: L-H. Han et al. Journal of Constructional Steel Research).

In order to examine the feasibility of using existing design codes to predict the ultimate strength of CFSST columns, the predictions from the Australian design code AS 5100, American code ANSI/AISC 360-05, Chinese code DBJ/T 13-51-2010 and Euro code 4 were compared by Uy et al to the test results. It was evident that all codes were conservative in predicting the load-carrying capacity of CFSST columns. For short columns under axial compression, AS 5100 gives the best predictions for circular columns, whilst DBJ/T offers the closest predictions for square columns. Meanwhile, all codes underestimate the capacity by 47–67% for short columns under compression and bending and about 11.1–25.5% for slender columns, respectively. Compared with a carbon steel tube, the amplitudes of local buckles in the stainless steel tubes are much higher. According to the experiment reported in, the axial shortening of a CFSST can reach as high as 20% without the observation of possible fracture of the stainless steel tube due to the high ductility of stainless steel. To allow the use of thin-walled stainless steel tubes.

D. lam, L.Gardner, M. Burdett (2010), conducted an experimental study to assess the behavior of concrete filled stainless steel elliptical sections with normal strength (30 MPa) and high strength (100 MPa) concrete. The elliptical section has one significant advantage over circular and square sections, since the majority of steel framed building consist of one way spanning floor system to withstand a large load and moment in major axis. A total of nine-stub column test have been performed to investigate the compressive behavior, six of them were concrete-filled and three were unfilled. The compressive response was found to be sensitive to both steel tube thickness and concrete strength, with higher tube thickness resulting in higher load-carrying capacity and enhanced ductility, and higher concrete strength improve load carrying capacity but reducing ductility.

2.3.4 Numerical Investigations

Numerical analysis is one of the most important tool to conduct the analytical study and it is very popular and effective to give a clear idea about the study. Number of numerical study with different parameter was conducted of CFSST columns by Ehab Ellobody (2007), M.F. Hassanein (2010), Dia & Lam (2010), Tao , Brian Uy, Fei-Yu Liaob, Lin-Hai Han (2011), Bambachn (2010).

Ehab Ellobody (2007) investigated the behavior and design of concrete-filled high strength stainless steel stiffened slender tube columns. A nonlinear finite element (FE) model for the analysis of the columns has been developed. The material nonlinearities of high strength stainless steel tubes and confined concrete have been carefully considered. The column strengths, deformed shapes and load–axial shortening behavior of the columns have been predicted using the FE model.

The results of the concrete-filled stiffened tube columns were compared with the results of the companion concrete filled unstiffened tube columns. Parametric study of 60 concrete-filled stainless steel stiffened and unstiffened slender tube columns of SHS and RHS having the overall depth-to-plate thickness (D/t) ratio ranging 60–160 as well as different concrete cylinder strengths ranging 20–100MPa was performed. It is shown that the concrete-filled stiffened slender tube columns offer a considerable increase in the column strength and ductility than the concrete-filled unstiffened slender tube columns.

The column strengths obtained from the FE analysis were compared with the design strengths predicted using the American and Australian/New Zealand specifications for stainless-steel and concrete structures. It is shown that the design strengths calculated using the American and Australian/New Zealand specifications are generally conservative for concrete-filled stainless steel stiffened tube columns having d/t ratio less than 45.5, whereas the design strengths were more conservative for columns having d/t ratio greater than or equal to 45.5 and for concrete-filled unstiffened slender tube columns investigated in this study. Hence, modification to the design rules specified in the American and Australian/New Zealand specifications was proposed for concrete-filled stainless steel stiffened slender tube columns having d/t ratio greater than or equal to 45.5 and for concrete-filled unstiffened tube columns. The design strengths predicted using the proposed modified equation are more accurate compared with the design strengths calculated using the American and Australian/New Zealand specifications.

M.F. Hassanein (2010) has done Numerical modeling of concrete-filled lean duplex slender stainless steel tubular stub columns. Here finite element modeling for concrete-filled lean duplex slender stainless steel tubular stub columns of Grade EN 1.4162 is presented in this paper. The paper is predominantly concerned with two parameters: cross-section shape and concrete compressive strength, which have not yet been investigated. The non-linear displacement analysis of the columns was constructed herein based on the confined concrete model provided by Hu et al. (2003) .The behavior of the columns was investigated using a range of concrete cylinder strengths (25-100 MPa). The overall depth-to-width ratios (aspect ratio) varied from 1.0 to 1.8. The depth-to-plate thickness ratio of the tube sections varied from 60 to 90. The concrete-filled lean duplex slender stainless steel tubular columns were subjected to uniform axial compression over the concrete and stainless steel tube to force the entire section to undergo the same deformations by blocking action. The ABAQUS 6.6 program, as a finite element package, is used in the current work. The results showed that the design rules specified in the ASCE are highly conservative for square and rectangular concrete-filled lean duplex slender stainless steel stub columns while they are conservative in the case of European specifications. Author, therefore, proposed that is accurately found to represent the behavior of concrete-filled lean duplex stainless steel tubular stub columns.

Dai and Lam (2010) investigated the axial compressive behavior of short concrete-filled elliptical steel columns using the ABAQUS/Standard solver and proposed a new confined concrete stress stain model for the concrete-filled elliptical steel hollow section. The accuracy of the simulation and the concrete stress strain model was verified experimentally. The stub columns tested consist of 150 to 75 elliptical hollow sections (EHSs) with three different wall thicknesses (4 mm, 5 mm and 6.3 mm) and concrete grades C30, C60 andC100. Author found that compressive behavior, which includes the ultimate load capacity, load versus end-shortening relationship and failure modes, were obtained from the numerical models and compared against the experimental results, and good agreements were obtained. This indicated that the proposed model could be used to predict the compressive characteristics of short concrete-filled elliptical steel columns.

Zhong Tao, Brian Uy, Fei-Yu Liao, Lin-Hai Han (2011) carried out Nonlinear analysis of concrete-filled square stainless steel stub columns under axial compression. Concrete-filled stainless steel tubes (CFSST) can be considered as a new and innovative kind of composite construction technique, and have the potential to be used extensively in civil engineering.

The paper employs a nonlinear analysis of square CFSST stub columns under axial compression. A three-dimensional nonlinear finite element (FE) model is developed using ABAQUS, where nonlinear material behavior, enhanced strength corner properties of steel, and initial geometric imperfections are included. Close agreement is achieved between the test and FE results in terms of load-deformation response and ultimate strength. In light of the numerical results, the behavior of stainless steel composite columns is compared with that of carbon steel composite columns. A simple model is proposed to calculate the ultimate strength of square CFSST stub columns.

Bambachn (2010) has done extensive research on design of hollow and concrete filled steel and stainless steel tubular columns for transverse impact loads. In this paper the study is done to investigate nominally identically sized stainless steel tubes, tested experimentally under the same conditions. Comparisons between the performance of the two materials are made. Both the steel and stainless steel tubular members, hollow and concrete filled, are then modeled numerically. The FE models are validated against the experiments, and subsequently extended to investigate the general behavior of such members when used as columns or other axially load bearing structures. The influences of axial preload, rotational restraint at the member ends, axial restraint, metal material properties and concrete filling, are investigated. In particular, their effect on the capacity of the members to absorb transverse impact energy. A general design procedure for metal tubular members with or without concrete filling subjected to transverse impact is developed by the author in a format aligned with current static structural steel specifications.

2.4 AISC Code Predicted Capacity

Composite columns are consisting of three different types of sections: (a) compact sections, (b) non compact sections and (c) slender sections. When the slenderness ratios are sufficiently small, the member can attain its full plastic moment, it is called Compact section. When the slenderness ratios are larger, the compression may buckle locally before gaining full plastic moment is called Non compact section. Slender section may defined as the slenderness ratios are sufficiently large, local buckling will occur before the yield stress of the material is reached.

Table: 2.1 Limiting

Width to Thickness Ratios for Compression Steel Elements in Composite Members Subject to Axial Compression (Source: AISC 360-10)

Description of Element	Width-Thickness Ratio	λ_p Compact/ Noncompact	λ_r Noncompact/ Slender	Maximum Permitted
Walls of Rectangular HSS and Boxes of Uniform Thickness	b/t	$2.26\sqrt{\frac{E}{F_y}}$	$3.00\sqrt{\frac{E}{F_y}}$	$5.00\sqrt{\frac{E}{F_y}}$
Round HSS	D/t	$\frac{0.15E}{F_y}$	$\frac{0.19E}{F_y}$	$\frac{0.31E}{F_y}$

Table: 2.2 Limiting Width-to-Thickness Ratios for Compression Steel Elements in Composite Members Subject to Flexure (Source: AISC 360-10)

Description of Element	Width-to-Thickness Ratio	λ_p Compact/ Noncompact	λ_r Noncompact/ Slender	Maximum Permitted
Flanges of Rectangular HSS and Boxes of Uniform Thickness	b/t	$2.26\sqrt{\frac{E}{F_y}}$	$3.00\sqrt{\frac{E}{F_y}}$	$5.00\sqrt{\frac{E}{F_y}}$
Webs of Rectangular HSS and Boxes of Uniform Thickness	h/t	$3.00\sqrt{\frac{E}{F_y}}$	$5.70\sqrt{\frac{E}{F_y}}$	$5.70\sqrt{\frac{E}{F_y}}$
Round HSS	D/t	$\frac{0.09E}{F_y}$	$\frac{0.31E}{F_y}$	$\frac{0.31E}{F_y}$

For compression, filled composite sections are classified as compact, non-compact or slender. For a section to qualify as compact, the maximum width-to-thickness ratio of its compression steel elements shall not exceed the limiting width-to-thickness ratio, λp, from Table 2.1. If the maximum width-to-thickness ratio of one or more steel compression elements exceeds λp, but does not exceed λr from Table 2.1, the filled composite section is non-compact. If the maximum width-to-thickness ratio of any compression steel element exceeds λr, the section is slender. The maximum permitted width-to-thickness ratio shall be as specified in the table. For flexure, filled composite sections are classified as compact, non-compact or slender. For a section to qualify as compact, the maximum width-to-thickness ratio of its compression steel elements shall not exceed the limiting width-to-thickness ratio, λp, from Table 2.2. If the maximum width-to-thickness ratio of one or more steel compression elements exceeds λp, but does not exceed λr from Table 2.2, the section is non-compact. If the width-to-thickness ratio of any steel element exceeds λr, the section is slender. The maximum permitted width-to-thickness ratio shall be as specified in the table.

(a) For compact sections

$$P_{no} = P_P \qquad 2.1$$

Were

$$P_p = F_y A_s + C_2 f_c' \left(A_c + A_{sr} \frac{E_s}{E_c}\right) \qquad 2.2$$

$$or \quad P_p = F_y A_s + 0.85 f_c' A_c \qquad 2.3$$

C_2 = 0.85 for rectangular sections and 0.95 for round sections.

(b) For noncompact sections

$$P_{no} = P_{nc} = P_p - \frac{P_p - P_y}{(\lambda_r - \lambda_p)^2}\left(\lambda - \lambda_p\right)^2 \qquad 2.4$$

Where λ, λ_p and λ_r are slenderness ratios

P_p is determined from Equation (2.3)

$$P_y = F_y A_s + 0.7 f_c' (A_c + A_{sr} \frac{E_s}{E_c}) \qquad 2.5$$

$$or \quad P_y = F_y A_s + 0.7 f_c' A_c \qquad 2.6$$

(c) For slender sections

$$P_{no} = P_{cr} = F_{cr} A_s + 0.7 f_c' (A_c + A_{sr} \frac{E_s}{E_c}) \qquad 2.7$$

$$P_{no} = P_{cr} = F_{cr} A_s + 0.7 f_c' A_c \qquad 2.8$$

Where

$$F_{cr} = \frac{9\, E_s}{(b/t)^2} \qquad 2.9$$

A_c	Area of concrete,
A_s	Cross-sectional area of steel section
A_{sr}	Area of continuous reinforcing bars
E_c	Modulus of elasticity of concrete
E_s	Modulus of elasticity of steel
F_{cr}	Critical stress,
F_y	Yield strength of structural steel shape
f'_c	Compressive stress of concrete
P_{no}	Nominal compressive strength of zero length
P_p	Nominal bearing strength
λ	Slenderness parameter
λ_p	Limiting slenderness parameter for compact element
λ_r	Limiting slenderness parameter for noncompact element

2.5 Limitations of AISC Code

(a) For the determination of the available strength, concrete shall have a compressive strength, f'_c, of not less than 3 ksi (21 MPa) nor more than 10 ksi (70 MPa) for normal weight concrete and not less than 3 ksi (21 MPa) nor more than 6 ksi (42MPa) for lightweight concrete.

(b) The specified minimum yield stress of structural steel and reinforcing bars used in calculating the strength of composite members shall not exceed 75 ksi (525MPa).

(c) For filled composite members, the cross-sectional area of the steel section shall comprise at least 1% of the total composite cross section.

2.6 Conclusions

Literature review presented in this chapter has made clear that limited experimental investigations were carried out on strength behaviour and failure modes of short and slender CFSST columns with normal strength (f'_c=21 MPa) to high strength (f'_c< 65 MPa) of concrete and structural steel strength 320 MPa to 650 MPa for concentric and eccentric loading conditions. A few numerical studies also have been done of CFSST column with concrete strength up to 100 MPa for both loading but not in vast way. Studies on CFSST columns using large cross sectional area and length are very limited. Very limited studies have been done to understand the behaviour of CFSST columns with high and ultra-high strength materials till now. Effects of several geometric parameters such as column slenderness ratio, depth to thickness ratio, load eccentricity ratio, high strength concrete comparison with code need to be explored. Code predicted capacity for high strength materials also need to be explored. In most of the codes, the upper limit for the strength of concrete is 70 MPa and for structural steel is 525 MPa. To understand the behavior of high strength materials, numerical investigation is the best way to explore the CFSST columns as it is less time consuming.

CHAPTER 3

EXPERIMENTAL INVESTIGATION OF CFSST COLUMN

3.1 Introduction

In this study an experimental investigation was performed to determine failure mode and load-deflection behavior of CFSST columns. For this purpose, Twenty four (24) CFSST columns in four (4) groups, each group containing six Specimens (3 square, 2 rectangular and 1 circular) were tested experimentally for concentric axial load. These columns were constructed with pre-casted sections. Among these, four groups of different cross sections were segregated. Each group contained 6 different cross sections of Stainless steel tubes. In each group three (3) of them were filled with concrete of different strength (30 MPa, 40 MPa and 50 MPa) and one was kept hollow. All of the test specimens were tested at the Solid Mechanics laboratory of Military Institute of Science and Technology (MIST). Failure modes, peak loads, experimental load deflection behavior (both axial and lateral) were examined in this study. The description of the test specimens, test setup, loading conditions and results obtained are presented in the following sections.

3.2 Test Program

The test program was done with different cross-sectional sizes as many as six of each four groups (based on concrete strength such as 30 MPa, 40 MPa and 50 MPa) comprising of one hollow batch with three filled batch each one with a different concrete strength was fabricated. The cross-sectional dimensions were different, though they fall in the broad classification of rectangular, square and circular. In total 24 different specimens were tested and the ultimate load carrying capacity and failure behavior were determined for concentric loading condition. Load versus axial shortening and load versus lateral deflection were also observed.

3.2.1 Test Specimen Description

The test specimens were different shape and size either concrete filled or hollow. Four different groups of specimens based on concrete strength with the square, rectangular and circular shape are taken for the experimental analysis are described in Table 3.1.

Table 3.1: Geometric and Mechanical Properties of Test Specimens

Shapes	Group ID	Breadth (mm)	Width (mm)	Depth (mm)	Type	fc′ (MPa)	Steel wall Thickness (mm)
Square **(50.8x50.8x152.4)**	Gp- 1	50.8	50.8	152.4	Filled	50	1.5
	Gp- 2				Filled	40	1.5
	Gp- 3				Filled	30	1.5
	Gp- 4				Hollow	-	1.5
Rectangular **(76.2x50.8x228.6)**	Gp- 1	76.2	50.8	228.6	Filled	50	1.5
	Gp- 2				Filled	40	1.5
	Gp- 3				Filled	30	1.5
	Gp- 4				Hollow	-	1.5
Rectangular **(101.6x50.8x304.8)**	Gp- 1	101.6	50.8	304.8	Filled	50	1.5
	Gp- 2				Filled	40	1.5
	Gp- 3				Filled	30	1.5
	Gp- 4				Hollow	-	1.5
Square **(76.2x76.2x228.6)**	Gp- 1	76.2	76.2	228.6	Filled	50	1.5
	Gp- 2				Filled	40	1.5
	Gp- 3				Filled	30	1.5
	Gp- 4				Hollow	-	1.5
Square **(63.5x63.5x190.5)**	Gp- 1	63.5	63.5	190.5	Filled	50	1.5
	Gp- 2				Filled	40	1.5
	Gp- 3				Filled	30	1.5
	Gp- 4				Hollow	-	1.5
Circular **(D_101.6x304.8)**	Gp- 1	Radius= 50.8 mm		304.8	Filled	50	1.5
	Gp- 2				Filled	40	1.5
	Gp- 3				Filled	30	1.5
	Gp- 4				Hollow	-	1.5

3.2.2. Introduction to Test Parameters

All the test specimens were designed to examine the behavior for concentric loading. CFSST columns were constructed with normal strength concrete for experimental investigation of their behavior and failure mode, as well as to evaluate their capacity against predicted capacity. Three types of sectional were used to evaluate the effect of sectional dimension on the capacity of CFSST column. Three types of concrete mix of 30 MPa, 40 MPa and 50 MPa were used. Details of geometric property and mechanical properties stated as in Table 3-1. CFSST column with same sectional dimension and different concrete strength were tested to find out the effect of concrete strength on the ultimate capacity of the CFSST. A hollow tube was tested to compare the capacities with concrete filled tube of same dimension. Load carrying capacity and failure behavior of these columns were determined individually.

3.3 Column Fabrication

Concrete filled tube column consisted of two parts that is the steel sections and concrete. The steel sections were prepared from cold formed stainless steel. The structural steel sections were fabricated with stainless steel from STEELECH industries Ltd, in Gazipur, Dhaka, Bangladesh. After fabrication of stainless-steel stub column, concrete of different strength was poured into the steel section.

3.3.1 Steel Section Fabrication

The stainless steel of stub columns were collected from The STEELECH industries Ltd, in Gazipur, Dhaka. The STEELECH industries Ltd is a professional dealer of stainless-steel tubes of different dimensions. Considering the availability and feasibility of experimental study, the cross sections were chosen and ordered them to manufacture accordingly. Then the tubes were cut down into required length segments of required number. Going to their workshop at Mirpur-11 and plates of 10 mm thickness made of mild steel were welded in the one end of the section. Then those were brought back to Concrete Lab and Concrete was filled to them with necessary tamping and vibrating and submerge under water in curing pool for

28 days. On completion of 28 days, they were pulled out of the water; extra concrete above was grinded and finally taken to them again for fixing the MS plate on the top side by welding. Base plates were connected to ensure the even distribution of load on all over the column section during testing. The procedure of mixing and preparing the specimens as Figure 3-1 shows all the steps in images.

3.3.2 Concrete Mix Design

The main interest of mix design were the properties of concrete strength and workability. Trial batches of all mixes were made to ensure the desired properties were obtained. All the 18 (eighteen) stub columns were casted with three (3) normal concrete strengths. From mix design total quantity of material were calculated for 18 (eighteen) CFSST columns and 9 (nine) cylinders shown in Table 3-3 and Table 3-4. Additional 9 (nine) cylinders of three mix ratios were trialed before casting the main columns. The concrete was made with locally available materials. The size of coarse and fine aggregate was 12.5mm and down grade. The cement used in concrete mix was Portland Composite Cement (PCC), CEM-I 52.5N Grade.

Table 3.2: Concrete Mix Design at Saturated Surface Dry (SSD) Condition (30 MPa)

Ser	Materials	Quantity		Ratio
		Weight (kg)	Volume (m^3)	
1.	Water	9.71	0.0097	0.4 (water cem)
2.	Cement	24.26	0.017	1
3.	Coarse Aggregates (Stone)	79.93	0.049	2.93
4.	Fine Aggregates (Sylhet Sand)	39.21	0.026	1.51

Table 3.3: Concrete Mix Design at Saturated Surface Dry (SSD) Condition (40 MPa).

Materials	Quantity		Ratio
	Weight (kg)	Volume (m^3)	
Water	21.563	0.0216	0.42 (water cem)
Cement	51.39	0.0356	1
Coarse Aggregates (Stone)	143.63	0.0894	2.507
Fine Aggregates (Sylhet Sand)	68.31	0.0441	1.244

Table 3.4: Concrete Mix Design at Saturated Surface Dry (SSD) Condition (50 MPa).

Materials	Quantity		Ratio
	Weight (kg)	Volume (m^3)	
Water	14.15	0.00142	0.41(water cem)
Cement	34.21	0.0238	1
Coarse Aggregates (Stone)	86.55	0.0539	2.25
Fine Aggregates (Sylhet Sand)	42.44	0.0275	1.15

Design was completed according to the ACI standard. Water cement ratio was 0.40, 0.42 and 0.41 for 30 MPa 40 MPa and 50 MPa strength concrete respectively which was determined using an empirical equation provided in ACI guideline. A slump value of 75 mm to 100 mm was found for this mix designs. From completed mix design, the obtained ratio of cement, fine aggregate and coarse aggregate is 1:1.51:2.93, 1:1.244:2.57 and1:1.15:2.25 for 30 MPa 40 MPa and 50 MPa normal concrete strength respectively.

3.3.3 Concrete Placement

All concrete was produced in the batching facility of the Concrete Laboratory at Military Institute of Science and Technology. In this experimental study, I had three groups (GP 1, GP 2 & GP 3) of filled tube columns were casted in three different days. The images of fabrication stages are given in figure 3.1.

(a) (b) (c) (d) (e) (f) (g)

Figure 3.1: Different stages of fabrication of the specimen.

Three groups of concrete cylinders (100 mm diameter, 200 mm height) were also cast with the column to determine the material properties of the concrete. A good standard in batching, placing, and vibration techniques were followed during concrete placement in all six CFSST columns.

3.4 Material Properties

Concrete filled stainless steel tube consists of steel section and concrete. To determine steel section's property coupon test was performed and to determine concrete strength, compressive strength test of concrete cylinder was performed. Total eighteen (18) numbers of cylinders were tested.

3.4.1 Stainless Steel Properties

All the plates used in sections were made from the same strength (Grade) plates. The properties (0.2% proof strength, ultimate strength) of the stainless-steel plates was determined from five coupons test from the spare steel sections. The tensile test of the steel plates was performed in the Solid Mechanics laboratory of Military Institute of Science and Technology (MIST). The result of the coupon test is given in Table 3.5. All the steel columns were built up sections, so the sections were connected through fillet welding. From the AISC specification criteria for compact, non-compact and slender column it was found that all the sections were compact sections. Stainless steel bars of 16 mm diameter were used. They welded with the steel plate to apply the load at desired eccentricity. Steel plates of 10 mm thickness were used at the ends of the columns. These steel plates were cut from the same steel sections of 250 MPa strength.

Table 3.5: Coupon Test Results

Coupon Bar Number	Proof Stress $\sigma_{0.2}$ MPa	Ultimate Stress σ_u MPa
C-1	**470.33**	**800**
C-2	**420.17**	**714**
C-3	**498.14**	**847**
C-4	**487.87**	**829**
C-5	**481.82**	**819**

"

Figure 3.2: Coupon test sample

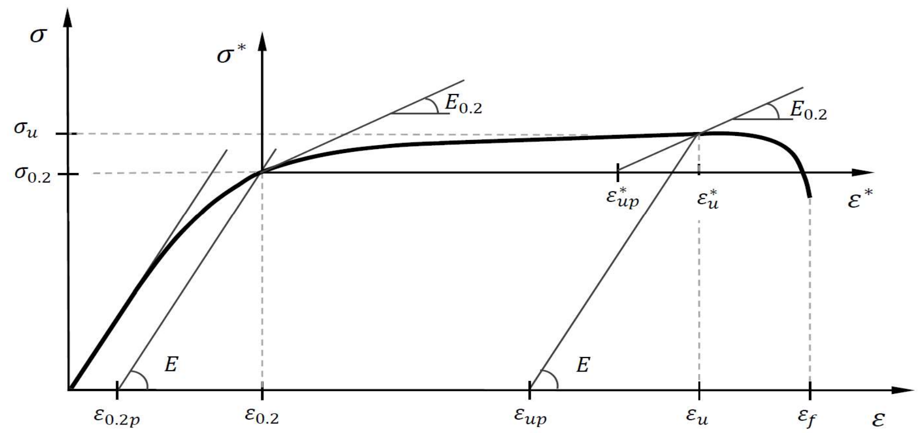

Figure 3.3: Typical 0.2% proof strength, ultimate strength curve. (Source: Arrayagoa , E. Reala , L. Gardner. Description of stress-strain curves for stainless steel alloys)

3.4.2 Concrete Properties

Three mix ratios were prepared to fabricate three groups of concrete filled tube (CFSST) columns. For determining the material properties, twelve (18) concrete cylinders of 100 mm diameter and 200 mm height were cast from each mix. Mix designs are represented by their respective predicted strengths namely 30 MPa 40 MPa and 50 MPa. Six (6) cylinders were prepared for each concrete strength of 30 MPa, 40 MPa and 50 MPa. After 24 hours from casting, cylinders were removed from molds and kept on the lime water for curing. Cylinders were tested in the compression-testing machine according to the ASTM Standard at Concrete Laboratory at Military Institute of Science and Technology on 7th, 21th & 28th day. Compressive strength of all cylinders are listed in Table 3.7 Average compressive strength of three groups of cylinders after 7 days is found 19.95 MPa, 27.95 MPa and 34.58 MPa for predicted strength 30 MPa 40 MPa and 50 MPa respectively. Among the other twelve (12) cylinders, six of each ratio was tested on the twenty first day for compressive strength. The average strength of cylinders after 21 days was found 26 MPa, 35.3 MPa and 44.14 MPa for predicted strength of 30 MPa, 40 MPa and 50 MPa respectively. The average compressive strength of three groups of cylinders after 28 days was found were found 29.15 MPa, 38.75 MPa and 48.54 MPa respectively. Observing the failure pattern, it was seen that cylinders of predicted strength 50 MPa failed primarily due to columnar failure or axial split failure and cylinders of predicted strength 30 MPa and 40 MPa failed mainly due to splitting and shear failure.

Table 3.6: Strengths of Different Concrete Cylinders of Different Age.

Desired Strength/ Gained Strength	30 MPa		40 MPa		50 MPa	
7 Day	19.6	20.3	27.6	28.3	33.95	35.21
21 Day	25.4	26.6	34.7	35.9	44.57	43.71
28 Day	28.6	29.7	38.3	39.1	49.01	48.07

Figure 3.4: Spliting and shear failure

Figure 3.5: Splitting and shear failure mode of 30 MPa concrete cylinders

Figure 3.6: Splitting and shear failure mode of 30 MPa concrete cylinders

3.5 Test Setup and Procedures

UTM (Universal Testing Machine) as well as the test specimens set up procedure is elaborated in subsequent steps.

3.5.1 Testing Machine and Data Acquisition System

The experimental investigations were carried out in MIST Mirpur. All tests were performed using a Universal Testing System (UTS) machine. All the specimen columns were tested using the UTM of Solid Mechanics Laboratory of MIST. The capacity of this UTM is 1000 KN.

Figure 3.7: Specimen setup on UTM

Figure 3.8: Test interface in the controller

Figure 3.9: Parameters at the controller interface

UTM load and stroke rates were verified before each test to ensure correct readings. For the tests carried out the data acquisition system used a PC running Blue hill data acquisition software. Load and corresponding displacements data were given in every 0.1 second interval for all the columns. The UTM instruments are frequently calibrated and verified according to a regular schedule. Real-time graphs of the key data were displayed during loading to assist in controlling the tests. The displacement-controlled rate was fixed to 1 mm/min for all the columns. As laboratory safety regulations do not allow anyone near the UTM while it is operating, so the photographs are taken before and after each test is done.

3.5.2 Setup and Instrumentation of Specimen

All the specimens were tested in concentric axial loading condition where the top and bottom were directly placed to UTM, and 10 mm thick mild steel was welded in both the sides to ensure equal loading in both concrete and steel. This represents fixed support in bottom and top end remain restrained in all side except vertical deformation on loading in top end. The columns were placed in the UTM and then centered. Before starting loading, a sufficient gap between column top and machine had provided. Considering all types of effects including failure of columns, a uniform stroke rate of 1 mm/ min was used throughout the loading in fourteen columns.

Figure 3.10: Test setup of specimen's top support and bottom support

Figure 3.11: Full test setup of specimen

CHAPTER-4

FINITE ELEMENT MODEL OF CFSST COLUMNS

4.1 Introduction

Experimental and analytical studies have been done by many researchers to understand the behaviour of the composite columns mainly from the 1960s. Composite columns have more advantages than the conventional reinforced concrete and steel structures, namely high speed of construction work resulted from the omission of framework and the reinforcing bars and low structural costs. In recent years, a number of researches had been conducted to study the impact behavior of the composite members through experimental and theoretical works and finite element analysis. Experimental research on composite column is not only time depending but also costly. On the other hand, due to development of digital computer and numerical techniques, the finite element method (FEM) has become very powerful analytical tool for structural analysis. Number of variations can be done by numerical analysis. Recently few researchers have conducted numerical program along with the experimental to study the behaviour of CFSST column and it was found that the numerical study very much comply with the experimental study.

In this study general purpose finite element software ABAQUS 14.4 is used to simulate the behaviour of CFSST columns. Total a no of 44 numerical models have been validated, out of them 20 model was validated against our own experimental results and 24 numerical models was validated against the result of recently published available renowned relevant papers. This chapter highlights the procedures to simulate these models. It is worth mentioning that the procedures mostly followed previous numerical study conducted by different researchers.

4.2 Element Selection

The CFSST columns are combination of two different materials, Stainless steel tube and core concrete. The core concrete and steel tube were modeled as 8-nodeed brick element (C3D8R) and 4-nodeed shell element (S4R), respectively (Figure 3.1). The S4R element has six degree of freedom per node and provides accurate results for elements having higher width-to-thickness ratio. The default number of integration points through the thickness of this element were five, which is sufficient for modelling the nonlinear material behaviour of the current problem under monotonic loading.

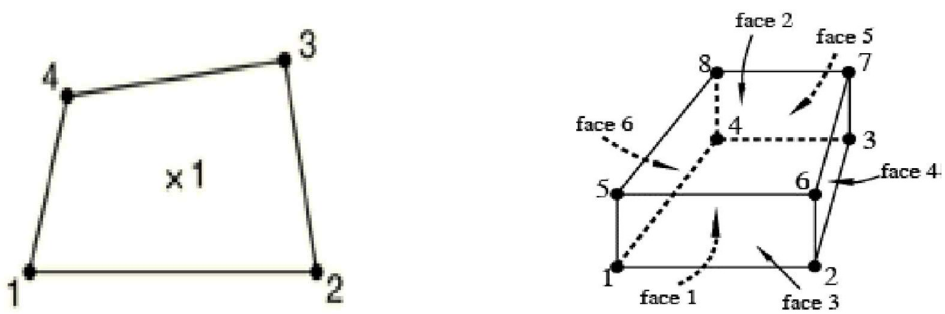

4-nodeed shell element

(a)

8-nodeed solid element

(b)

Figure 4.1: Finite elements used in the numerical simulation, (a) S4R Shell element; (b) C3D8R brick element.

4.3 Interaction between Stainless Steel and Concrete

Surface-to-surface contact is used to simulate the interaction between inner surface of stainless steel tube and outer surface of core concrete. Two different interface property is provided for normal and tangential direction. “Hard contact” in the normal direction was specified for the interface in normal direction which allows separation in tension and no penetration in compression. For tangential interface, Columb friction model available in ABAQUS was used. A sensitivity analysis was conducted to find out the influence of coefficient of friction in overall behaviour of CFSST column. Coefficient of friction was taken 0.25 into the analysis, as it is comparatively smoother than the carbon steel. It was found through the sensitivity analysis that the influence of coefficient of friction is insignificant. As the outer steel and core concrete are loaded simultaneously in CFSST column, there is little or no slip between the surfaces. Based on the above statement the result of the sensitivity analysis can be justified. The surface-to-surface contact formulation generates individual contact constraints using a master-slave approach (ABAQUS Documentation). As steel is stiffer, steel inner surface is considered as master surface and concrete surface is considered as slave surface. It has been well documented that initial local imperfections and residual stresses have apparent influence on the behaviour of hollow tubes. For CFST stub columns, however, the effects of local imperfections and residual stresses are minimized by concrete filling, and were therefore ignored in the current FE simulation.

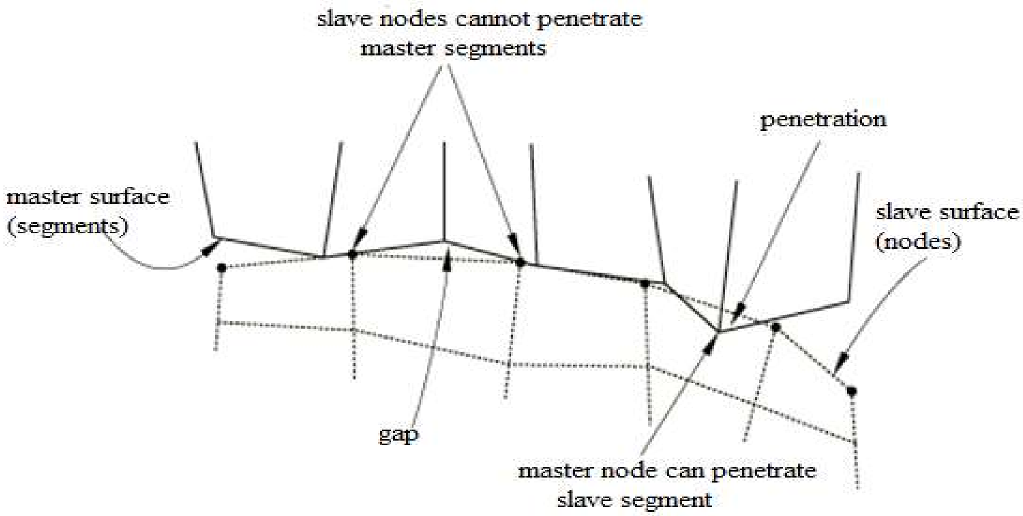

Figure 4.2 Master and slave contact pair

4.4 Sensitivity Analysis

Mesh convergence studies have been conducted to determine optimal FE mesh that provides relatively accurate solution with low computational time. To do so, a specimen of 500 mm x 500 mm of 1500 mm length (Chen et al.2012) was taken as base specimen. Three types of mesh size have been used here to find out the optimum mesh size. From the sensitivity analysis it is found that medium and fine mesh gives similar results (Table 3:1). However, medium mesh size is considered to be the optimum mesh size based on both accuracy and computational cost. Element size across the cross-section have been chosen as B/15(Medium Mesh), where B is the overall width of the steel tube. The ratio of width/breath to length was taken as 1:3.

Table 4:1 Sensitivity Analysis

Mesh Name	Element Size	Number of Elements	Num (kN)	Exp (kN)	$\frac{P_{Num}}{P_{Exp}}$	Time (Sec)
Coarse	B/10	1400	16770	16500	1.01	29
Medium	B/15	4275	16664	16500	1.00	79
Fine	B/20	9600	16507	16500	1.00	229

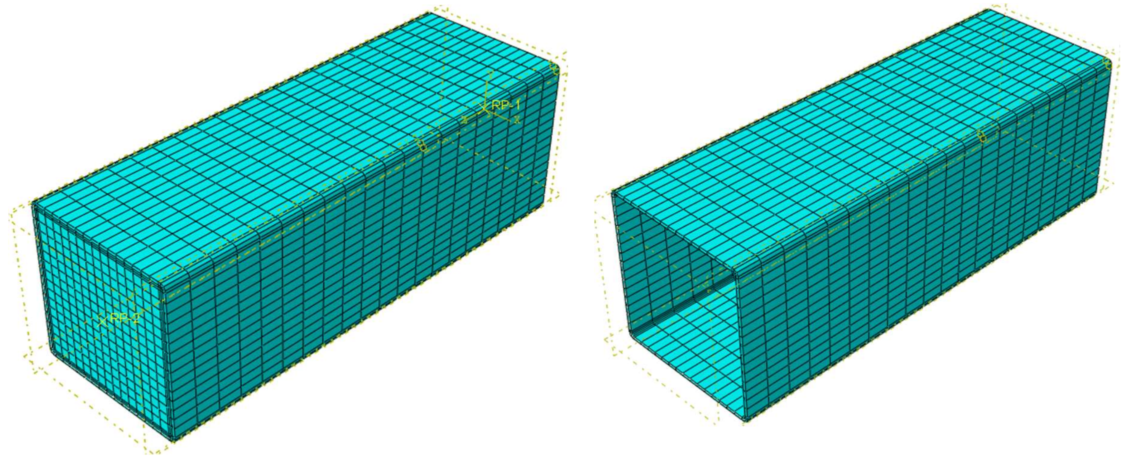

(a) (b)

Figure 4.3 Meshing technique for steel and composite sections, (a) Composite section; (b) Stainless steel section

4.5. Material Modeling of Stainless Steel

Stainless steel and concrete are the materials used in FE model for numerical investigation. Plastic properties for these materials shown in Table was used in the FE model. Elasto-plastic material model is used to simulate the behaviour of square section CFSST columns. The damage plasticity model in ABAQUS was used to simulate the concrete material behaviour in the composite columns.

4.5.1 Stainless Steel

To develop a suitable model for stainless steel is very crucial in modelling CFSST columns since the material behaviour of stainless steel is quite different from that of carbon steel. It is well known that the nonlinear stress (σ)–strain (ε) curves of stainless steel are of a "round house" type. To describe a full-range stress–strain relationship was proposed by Rasmussen, in which the Ramberg–Osgood expression was used for the range up to the 0.2% proof stress, and a new expression given for higher strains.

$$\varepsilon = \frac{\sigma}{E_0} + 0.002\left(\frac{\sigma}{\sigma_{0.2}}\right)^n \quad \sigma \leq \sigma 0.2 \tag{4.1}$$

$$n = \frac{ln(20)}{ln(\sigma_{0.2} / \sigma_{0.01})}. \tag{4.2}$$

In which E_0 is the initial elastic modulus, and $\sigma_{0.2}$ is the 0.2% proof stress. n is the strain-hardening exponent determined by $\sigma_{0.2}$ and the 0.01% proof stress $\sigma_{0.01}$.

$$\varepsilon = \frac{\sigma - \sigma_{0.2}}{E_{0.2}} + \varepsilon_u \left(\frac{\sigma - \sigma_{0.2}}{\sigma_u - \sigma_{0.2}} \right)^m + \varepsilon_{0.2}, \sigma > \sigma_{0.2} \qquad 4.3$$

in which

$$E_{0.2} = \frac{E_0}{1 + 0.002n/e}$$

$$e = \frac{\sigma_{0.2}}{E_0}$$

$$\frac{\sigma_{0.2}}{\sigma_u} = \frac{0.2 + 185e}{1 - 0.0375(n-5)}$$

$$\varepsilon_u = 1 - \frac{\sigma_{0.2}}{\sigma_u}$$

$$m = 1 + 3.5\frac{\sigma_{0.2}}{\sigma_u}$$

$$\varepsilon_{0.2} = \frac{\sigma_{0.2}}{E_0} + 0.002.$$

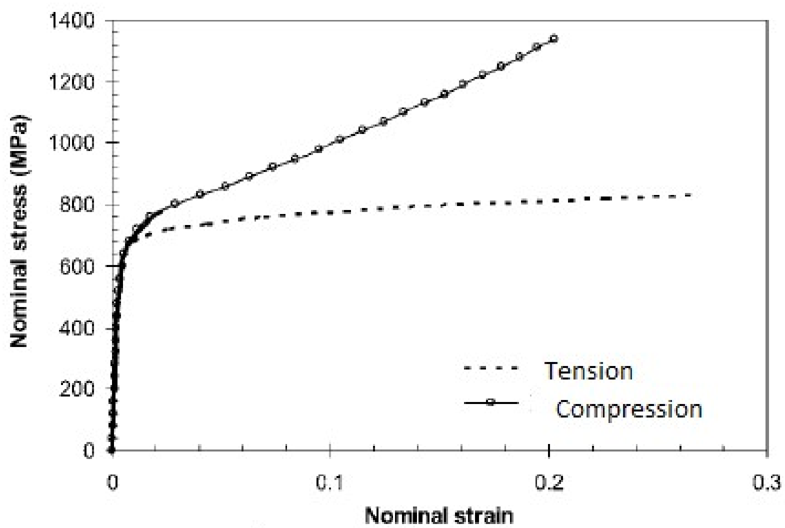

Figure 4.4: Full stress strain curves

Therefore, it is seen that only the three basic Ramberg–Osgood parameters (E0, $\sigma_{0.2}$, and n) are needed in the Rasmussen's model to determine the full-range stress–strain relationship.

4.6 Material Modeling of Concrete

Concrete is confined by steel tube in CFSST column. Strength and ductility is increased due to confinement of steel tube at time of applying load on CFSST column. This is known as "composite action" between the steel tube and concrete. Due to confinement by steel tube, concrete is in a tri-axial stress state and the steel is in a biaxial state after interaction between the two components.

4.6.1 Concrete Damaged Plasticity Model

The concrete damaged plasticity model in ABAQUS was used to simulate the behavior of concrete into CFSST columns. Damage variables were not defined due to monotonic loading. Therefore, concrete nonlinearity was modeled as plasticity only. In this model, key material parameters to be determined include the ratio of the second stress invariant on the tensile meridian to that on the compressive meridian (K_c), dilation angle (ψ), and strain hardening/softening rule. Other parameters include the modulus of elasticity (E_c), flow potential eccentricity (e), ratio of the compressive strength under biaxial loading to uniaxial compressive strength (f_{b0}/f'_c), viscosity parameter and tensile behaviour of concrete. For the FE model presented by Han et al.(2007), constant values of 30°, 0.1, 1.16 and 2/3 were used for ψ, e, K_c and f_{b0}/f'_c, respectively. The empirical Equation (3.1) recommended in ACI 318 was adopted to calculate E_c, where f'_c is in MPa. Default values of 0.1 and 0 were used for the flow potential eccentricity and viscosity parameter, respectively. These two parameters have no significant influence on the prediction accuracy.

$$E_c = 4700\sqrt{f'_c} \qquad 4.4$$

Test results of equibiaxial concrete strength (f_{b0}) are still very scarce. Based on test data collected from 14 references, Papanikolaou and Kappos (2007) proposed the following equation to predict the ratio of f_{b0}/f'_c:

$$f_{b0}/f'_c = 1.5\,(f'_c)^{-0.075} \qquad 4.5$$

For concrete strength f'_c is 30 MPa, f_{b0}/f'_c is 1.162 and for increasing f'_c to 100 MPa, f_{b0}/f'_c drops to 1.062.

Fracture energy (G_F) needs to be defined in ABAQUS. In this model, the uniaxial tensile response was assumed to be linear until the tensile strength of concrete was reached, and taken as $0.1f'_c$.

$$G_F = (0.0469d^2_{max} - 0.5d_{max} + 26)\,(f'_c/10)^{0.7}\ \text{N/m} \qquad 4.6$$

where f'_c is in MPa, d_{max} is the maximum coarse aggregate size in mm. If d_{max} had not been reported in a reference, then taken as 20 mm.

4.6.2 Compressive Meridian (Kc)

The compressive meridian (K_c) is the parameters for determining the yield surface of concrete plasticity model. The range of K_c varies from 0.5 to 1. The default value of K_c was used 2/3 in this ABAQUS model. A sensitivity analysis was carried out to investigate the influence of Kc on σ–ε curves of two specimens tested by Tomii et al. (1977).The value was found 0.725 to 0.703 for f'_c from 30 MPa to 100 MPa. It was observed that the compressive meridian (K_c) decreases with the increase of concrete compressive strength (f'_c).

4.6.3 Dilation Angle (ψ)

To define the plastic flow potential, dilation angle (ψ) is the important parameters for ABAQUS. It's allowable value ranges from 0° to 56°. Maximum researchers taken this value of 20° or 30° for confined concrete. Two specimens tested by Tomii et al.(1977) considering four different ψ values of 0.01°, 20°, 30° and 40°. Since ψ cannot be taken as 0 in ABAQUS, a small value of 0.01° was used to represent this level. Stronger interactions are developed between the steel tube and concrete with the increasing of ψ value. In square column, ψ has little influence and not so sensitive on the σ–ε curve if ψ is greater than 20°. The value of dilation angle (ψ) 40° gives the best prediction of the ultimate strength for rectangular columns.

4.6.4 Strain Hardening/Softening Rule

It is believed that there is negligible interaction between the steel tube and concrete in the initial loading stage for CFSST columns under axial compression. A small gap may occur between the steel tube and concrete due to the difference in Poisson's ratio of these two materials. As axial strain increases, the lateral expansion of the concrete gradually becomes greater than the expansion of the steel until the two components are in contact again. After that, contact pressure and interaction develop between the steel tube and concrete. This mechanism highlights the complexity of the interaction in CFSST columns. It is very difficult to measure the lateral expansion and confining pressure of concrete in a steel tube during the loading process. For this reason, no accurate model is available till now to describe the axial strain lateral strain relationship of concrete in CFSST columns. Based on numerical tests, researchers proposed different compressive σ–ε models to be used for FE modelling of concrete confined by steel tubes. These models can be used to determine the strain hardening/softening function directly.

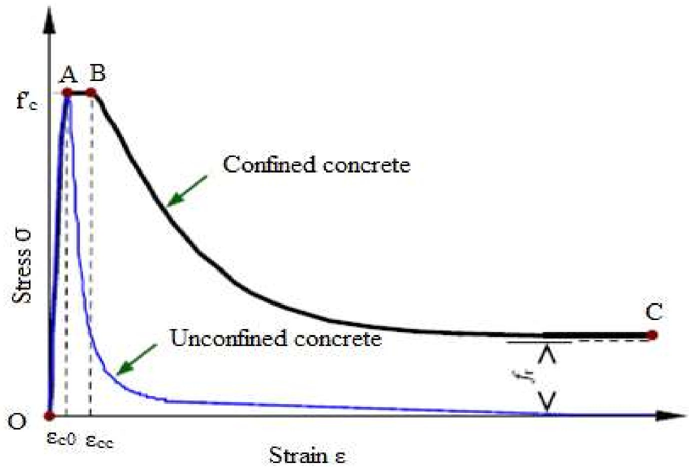

Figure 4.5 Stress–strain model proposed for confined concrete.

A new three-stage model was proposed by Han et al. (2007) to represent the strain hardening/softening rule of concrete confined by steel tubes, as shown in Figure 3.5. In the initial stage (from Point O to Point A), there is no or very little interaction between the steel tube and concrete. Therefore, the ascending branch of the stress–strain relationship of unconfined concrete is appropriate to be used to represent the curve OA until the peak strength f'_c is reached. After that, a plateau (from Point A to Point B) is included to represent the increased peak strain of concrete from confinement. During this stage, any strength increase of concrete from confinement will be captured in the simulation through the interaction between the steel tube and concrete. Beyond Point B, a softening portion with increased ductility resulting from confinement is defined. A model proposed by Samani and Attard (2012) is used to describe the ascending curve OA:

$$\frac{\sigma}{f'c} = \frac{AX+BX}{1+(A-2)X+(B+1)X^2} \qquad 0<\varepsilon\leq\varepsilon_{c0} \qquad 4.7$$

Where $X = \varepsilon/\varepsilon_{c0}$, $A= E_c\varepsilon_{c0}/f'c$ and $B= \{(A-1)^2/0.55\}-1$

The strain at peak stress under uniaxial compression ε_{c0} is calculated according to the relationship in Equation (3.5). This equation was proposed by De Nicolo et al. (1994) based on regression analysis of uniaxial compression tests results from seventeen references, in which f'_c ranged from 10 MPa to 100 MPa.

$$\varepsilon_{c0} = 0.00076 + \sqrt{(0.626 f'c - 4.33) \times 10^{-7}} \qquad 4.8$$

Where f'_c is expressed in MPa.

The strain at Point B (ε_{cc}) for the concrete model is determined by the following equation proposed by Samani and Attard (2012):

$$\frac{\varepsilon_{cc}}{\varepsilon_{co}} = e^{k} \qquad 4.9$$

$$k = (2.9224 - 0.00367\, f'_c)\, (f_B/f'_c)^{0.3124+0.002f'c}$$

Where f_B is the confining stress provided to the concrete at Point B.

For rectangular CFST columns, the concrete core is subjected to uneven confinement, and f_l at the corners will be higher than those at other parts. It is found that a reduction factor of 0.25 can be applied for rectangular CFSST columns and reasonable N–ε curves can be obtained. Therefore, f_B determining for rectangular CFST from Equation (3.7) can be viewed as an equivalent confining stress.

$$f_B = \frac{0.25 \cdot \left(1 + 0.027 f_y\right) \cdot e^{\frac{-0.02\sqrt{B^2+D^2}}{t}}}{1 + 1.6e^{-10} \cdot (f'_c)^{4.8}} \quad \text{(Rectangular)} \qquad 4.10$$

$$f_B = \frac{\left(1 + 0.027 f_y\right) \cdot e^{-0.02\frac{D}{t}}}{1 + 1.6e^{-10} \cdot (f'_c)^{4.8}} \quad \text{(Circular)} \qquad 4.11$$

For the descending branch of the concrete model (BC) shown in Figure 3.5, an exponential function proposed by Binici (2005) was used, which is defined by:

$$\sigma = f_r + (f'_c - f_r)\exp[-\{(\varepsilon - \varepsilon_{cc})/\alpha\}^{\beta}] \qquad \varepsilon \leq \varepsilon_{cc} \qquad 4.12$$

in which f_r is the residual stress as shown in Figure 3.5; α and β are parameters determining the shape of the softening branch. The expression for f_r is proposed for rectangular CFST as:

$$f_r = 0.1 f'_c \quad \text{(Rectangular)} \qquad 4.13$$

$$f_r = 0.7\left(1 - e^{-1.38\xi_c}\right) f'_c \leq 0.25 f'_c \quad \text{(Circular)} \qquad 4.14$$

and the parameter α is determined as:

$$\alpha = 0.005 + 0.0075\xi_c \quad \text{(Rectangular)} \qquad 4.15$$

$$\alpha = 0.04 - \frac{0.036}{1 + e^{6.08\xi_c - 3.49}} \quad \text{(Circular)} \qquad 4.16$$

Average value of β can be taken as 0.92 for rectangular columns. It should be noted that f_r, α and β cannot be derived from tests directly. Hence, different trial values were used until best-fit values were obtained to ensure predicted N–ε curves match with measured curves. It was found that f_r and α can be expressed as functions of ξ_c. where $\xi_c = \frac{A_s \cdot \sigma_{0.2}}{A_c \cdot f_{ck}} = \alpha \cdot \frac{\sigma_{0.2}}{f_{ck}}$ and equation (4.14), (4.15) and (3.16) were then developed on the basis of regression analysis.

4.7 End Boundary Conditions

Each point has six degrees of freedom. Three transitional and three rotational. The end boundary conditions in the FE model was defined in such a way to comply with that applied in the experimental setup. The boundary conditions applied in the FE model to simulate the conditions for concentrically and eccentrically loaded specimens are shown in Figure 3.6. In concentrically loaded column tests, the bottom end of the column was fixed and the axial load was applied through rigid body reference node at the center of the top end of the column. The rotations and horizontal translations at the top surface were fixed. Since the load is applied at the top the vertical restraint was released. The axial load was applied using a displacement control technique. In the finite element model for eccentrically loaded test specimens, rotations allowed about corresponding axis of eccentricity. A rigid body reference node is defined on the top of the column to apply displacement.

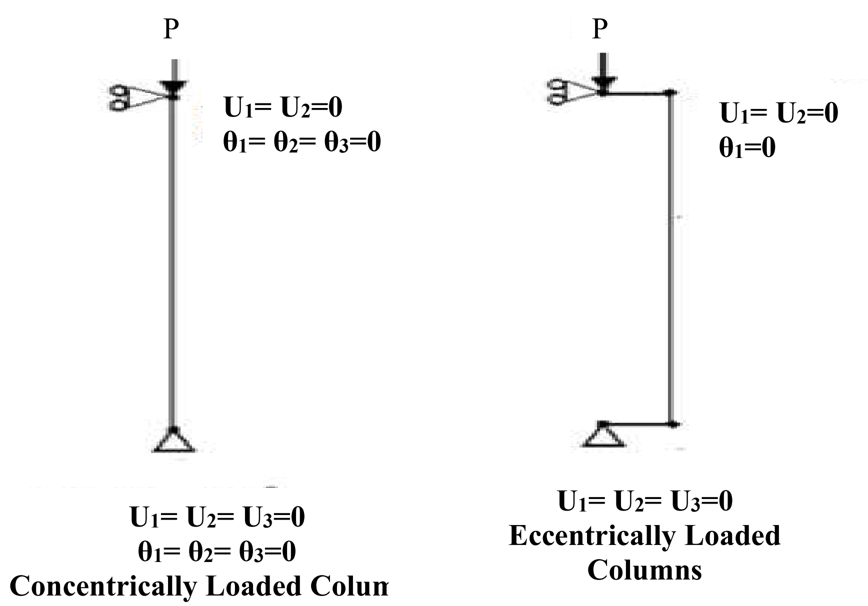

Figure 4.6 Load and solution strategy

4.8 Solving Techniques

Two distinctive methods are used to solve finite element problems, implicit and explicit. The implicit method solves for static or dynamic equilibrium, while the explicit method solves transient dynamic response using explicit direct-integration procedures. In the implicit method, each increment must reach convergence. Because of the presence of a large number of contact surfaces in the connection model assembly, convergence difficulties may occur in this method, while the explicit solver might exhibit fewer convergence difficulties. It is inferred that convergence is not an issue in the explicit numerical integration solution scheme; however, the results might be less reliable than using the implicit solver. Therefore, the results of the explicit solver should be verified closely. The implicit method has been selected for the research and solution strategy, Static (General).

4.9 Newton Raphson and Modified Newton Raphson Methods

The basic approach used in ABAQUS/Standard to solve nonlinear equations is Newton-Raphson iterative method. The solution procedure is shown in Figure 3.7. The solution seeks equilibrium through a horizontal path at a constant load vector. In this method the stiffness matrix ideally is updated at the end of every iteration. Since the major computational cost per iteration in Newton-Raphson iterations lies in the calculation decomposition of the tangent stiffness matrix developed at the beginning of a time step for all iterations within the time step, the solution path followed in a modified Newton-Raphson iterative method as illustrated in Figure 3.8. However, both methods failed to converge in the neighborhood of unstable responses such as near the ultimate load point.

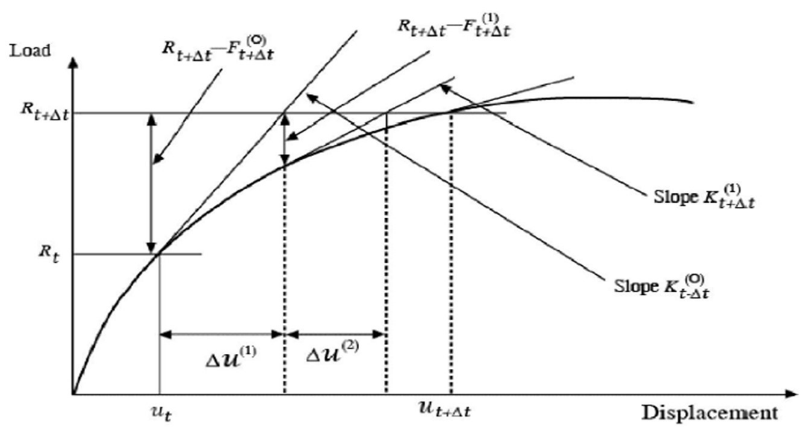

Figure 4.7 Newton-Raphson iterative method

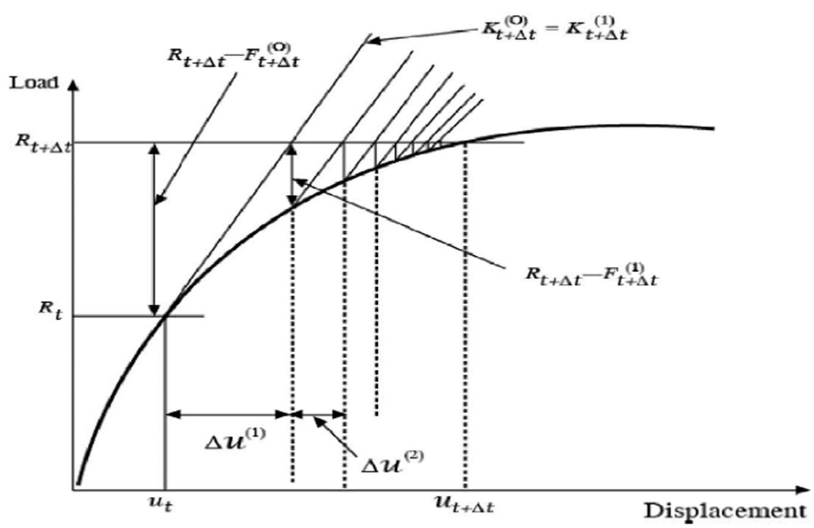

Figure 4.8 Modified Newton-Raphson iterative method

4.10 Conclusions

3D finite element model has been developed to understand the behavior of CFSST column in this chapter using the FE software ABAQUS (6.14). The concrete core was modeled with 8-nodeed brick element (C3D8R) with reduced integration and the steel tube was modeled with 4-nodeed shell element (S4R) with reduced integration. A validation study has been conducted in which the results of the FE models were compared with those of previous experimental studies. Geometric and mechanical nonlinearities are included in the FE model. The selection of the element types and mesh size are based on the behaviour of these columns which is obtained from sensitivity analysis. The concrete damaged plasticity model in ABAQUS was used to simulate the behavior of concrete into CFSST columns and steel was considered elastic-perfectly plastic model and the solution strategy was used Static (General).

CHAPTER-5

COMPARISON BETWEEN EXPERIMENTAL AND NUMERICAL RESULTS

5.1 Introduction

A comparative study was carried out to verify the numerical results with the experimental results which have been presented in this chapter. Experimental results was obtained from current experimental study in MIST Laboratory and more few available experimental results from recently published data in different journals. Numerical results were obtained from 3D nonlinear finite element analysis using ABAQUS finite element method. The numerical simulations were performed on a wide variety of CFSST columns with different geometric and material properties as experiential investigation was done. Experimental data of CFSST test columns results were analyzed to validate the numerical results with the experimental findings for concentric loads. The descriptions of the geometric and material properties of these test specimens are also presented in this Chapter. The comparisons are carried out on axial load capacity, axial strain, load versus deflection behaviour and modes of failure obtained from experimental and numerical studies. In addition, the developed FE model was used to predict the individual contributions of steel and concrete to the total load carrying capacity of the CFSST column.

5.2 Concentrically Loaded Columns

FE model of CFSST test specimen's column has been developed and simulated numerically for comparing the load deflection behavior of experimental data. The specimens varied in their size and shape (Square, Rectangular and Circular) and material properties (concrete strength 30, 40 and 50 MPa). Comparison between the experimental and numerical load deflection behaviour and ultimate capacities of stated sections and failure pattern are presented in the subsequent sections. Axial compressive strength, axial deformation and failure behavior were observed and recorded for each CFSST columns specimen experimentally and numerically. The experimental and numerical load deflection behavior of the column shown in Figure 5.1 & 5.2. It was observed that FE model can predict the experimental behaviour of CFSST columns with good accuracy in columns groups. However, the axial capacity and peak strain of these columns obtained from the numerical analysis matched very well with the corresponding experimental results.

The mean value of experimental-to-numerical peak load ratio, P_{exp}/P_{num} and experimental-to-numerical average axial strain at peak load, $\varepsilon_{exp}/\varepsilon_{num}$, were compared for all groups of columns. It is observed that the mean value and the standard deviation of the ultimate load ratio and corresponding strain ratio of numerical and experimental results for the two groups of test columns are reasonable. This indicates the excellent performance of the FE model in predicting the ultimate capacity of FEC columns with three different strength of concrete.

5.3 Comparison Between Current Experimental Results and FE Analysis.

Experimental analytical results from 24 specimens are compared with the numerical results (FE Analysis) of same section to verify the accuracy is stated in subsequent paragraphs.

5.3.1 Materials Properties

Material properties of concrete and stainless steel used in the experimental study is shown in Table-5.1.

Table-5.1 Materials Properties

Sl/no	Specimens Designation	Properties of Concrete			Properties of Stainless Steel		
		E_c (MPa)	f_c' (MPa)	ν	E_0 (MPa)	$\sigma_{0.2}$ (MPa)	n
1	Hollow	-	-	-	198000	471	3.5
2	C30	25375	29.15	0.2	198000	471	3.5
3	C40	29257	38.76	0.2	198000	471	3.5
4	C50	32745	48.54	0.2	198000	471	3.5

All the test specimens were designed to examine the behavior for concentric loading. CFSST columns were constructed with normal strength concrete for investigating their behavior and failure mode, as well as to evaluate their capacity against predicted capacity. Three types (Square, Rectangular and Circular) of sectional dimensions were used to evaluate the effect of sectional dimension on the capacity of CFSST column. Three types of concrete mix of 30 MPa 40 MPa and 50 MPa were used. Details of geometric and mechanical properties are given in Table 5.1. CFSST column with same sectional dimension and different concrete strength were tested to find out the effect of concrete strength on the ultimate capacity of the CFSST. A hollow tube was tested to compare the capacities with concrete filled tube of same dimension. Load carrying capacity and failure behavior of these columns were determined individually.

5.3.2 Experimental and Numerical Behavior of CFSST Column.

Figure 5.1 shows the axial load (N) versus axial strain (ε) curves for different types of CFSST columns. In this figure a comparative study has been shown between the numerically predicted load carrying pattern and that of the experimental test behavior of the same sectional properties. Here in this experimental study four groups of specimens with same sections of three concrete filled with 29.15 MPa, 38.75 MPa, 48.54 MPa strength concrete and one hollow stainless-steel stub columns were examined and compare with the exactly same sections and properties analyzed numerically. Comparison of test data and numerically predicted data is inserted in the following Table of 5.2.

Table 5.2 Comparison of Experimental and Numerical Results of Varying Concrete Strength.

Ser No	Specimen Designation	Conc Strength f_c' MPa	Peak axial load P_{Exp} (kN)	P_{Num} (kN)	P_{Exp}/P_{Num}	Experimental Peak load Strain $\varepsilon_{exp}(\mu_\varepsilon)$	Numerical Peak load Strain $\varepsilon_{num}(\mu_\varepsilon)$	$\varepsilon_{exp}/\varepsilon_{num}$
1	SC_50.8x50.8	Hollow	129	124	1.040	6889	6561	1.049
		30	184	189	0.974	6653	6168	1.0786
		40	223	202	1.089	6070	6457	0.940
		50	249	238	1.046	6441	6272	1.027
2	SC_63.5x63.5	Hollow	151	142	1.063	5578	5526	1.01
		30	277	256	1.082	5521	5517	1.00
		40	293	289	1.014	6210	5935	1.046
		50	356	328	1.085	6019	5926	1.015
3	SC_76.2x76.2	Hollow	168	176	0.955	4573	4486	1.019
		30	391	358	1.092	4736	4809	0.985
		40	423	411	1.029	4956	4989	0.993
		50	492	481	1.023	5021	5177	0.969
4	SC_76.2x50.8	Hollow	135	132	1.023	4181	4097	1.021
		30	265	254	1.043	4824	4729	1.020
		40	299	298	0.997	4773	4767	1.001
		50	355	344	1.032	5236	4961	1.055
5	SC_101.6x50.8	Hollow	134	128	1.047	3345	3451	0.969
		30	331	298	1.111	3465	3403	1.018
		40	363	340	1.068	3561	3501	1.017
		50	396	383	1.034	3458	3507	0.986
6	SC_Dia_101.6	Hollow	177	173	1.023	11429	12802	0.893
		30	476	469	1.015	8819	6609	1.334
		40	550	534	1.030	12278	9250	1.327
		50	657	633	1.038	7815	6922	1.129

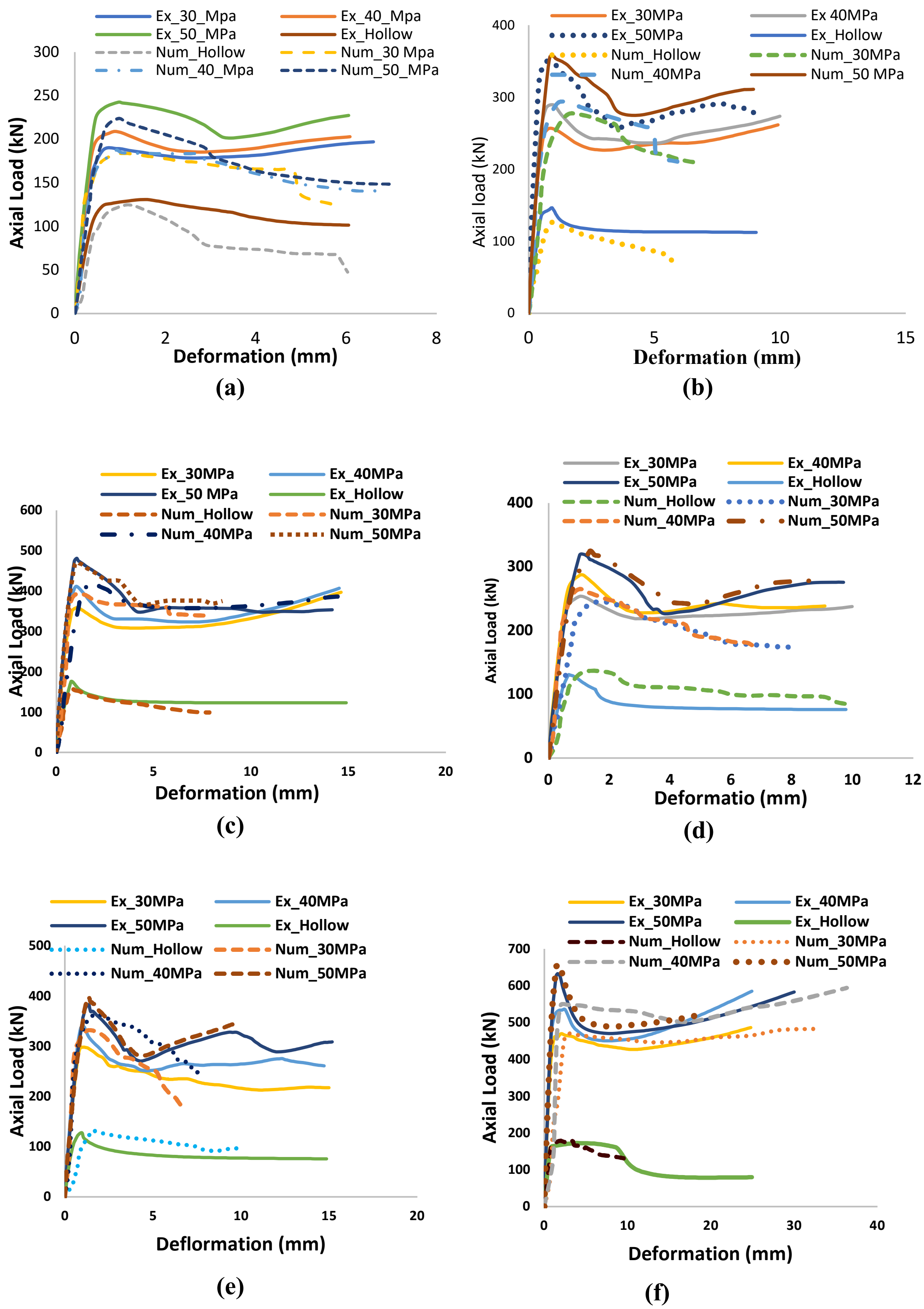

Figure 5.1: Experimental and numerical behaviour of column groups, axial load vs deformation, (a) SC_50.8x50.8; (b) SC_63.5x63.5; (c) SC 76.2x76.2; (d) SC 76.2x50.8; (e) SC_101.2x50.8; (f) SC_Dia_101.6

Numerical investigation data was compared with experimental data in Table 5.2 which presents the maximum axial compressive load and corresponding strain of the experimental tests. From comparison it is experienced that the numerical models can accurately predict the experimental axial compressive load and peak strain. The ratio of the numerical to experimental capacities, P_{exp}/P_{num} ranges from 0.927 to 1.092 and corresponding standard deviation 0.0034 which indicates the excellent performance of FE model with the accuracy of 0.996 in predicting the ultimate capacity of the FEC columns strength for concentrically loaded conditions. Again, the ratio of the numerical to experimental average axial strain at peak load, $\varepsilon_{num}/\varepsilon_{exp}$ ranges from 0.893 to 1.334 and the corresponding standard deviations 0.0098 which indicate the accuracy of 0.99. Thereby the FE model analysis are capable of predicting the ultimate capacity and peak strain of CFSST columns with good accuracy.

5.4 Comparison between Tao-2011 Experiment Result and FE Analysis.

Experimental and numerical data of Tao et al 2011 are compared with the current numerical analysis with same geometrical and mechanical properties to verify the FE analysis as follows.

5.4.1 Material Properties

Geometrical and Mechanical properties of of stainless steel and concrete of test specimens taken by Tao et al. stated as follows:

Table 5.3 Geometrical and Mechanical Properties of Test Specimens (Tao et al-2011).

Sl no	Specimens Designation (Tao et al)	Dimension (Square Column) B x t x L (mm)	Properties of Stainless Steel			Properties of Concrete		
			E_c (MPa)	f_c' (MPa)	ν	E_0 (MPa)	$\sigma_{0.2}$ (MPa)	n
1	S20-50x3-A	51x2.85x150	21795	21.5	0.2	207900	440	8.2
2	S20-100x5-A	101x5.05x300	21795	21.5	0.2	202100	435	7
3	S30-100x3-A	101x2.85x300	27765	34.9	0.2	195700	358	8.3
4	S30-150x3A	152x2.85x450	27765	34.9	0.2	192600	268	6.8
5	SHS1C40	150.5x5.83x450	32084	46.6	0.2	194000	497	3
6	SHS-5-C60	100x4.9x300	34216	53	0.2	180000	458	3.7
7	S30-100x5B	101x5.05x300	27765	34.9	0.2	202100	435	7
8	C30-150x1.6B	152.4x1.6x450	25742	30	0.2	195000	279	7

5.4.2 Comparison of Tao et al. 2011 Experimental and Numerical Results with Current Numerical Results

Tao et al. 2011 experimental and numerical Peak load carrying capacity of varying concrete strength and stainless-steel section inserted in the Table 5.4. Experimental peak load stain and numerical peak load strain also shown in following table.

Table 5.4: Comparison of Experimental (Tao et al.) and Numerical Results of Varying Concrete Strength and Section

Sl No	Specimen Designation	Conc Strength f_c'(MPa)	Peak axial load		P_{Exp} /P_{Num}	Exp Peak load Strain $\varepsilon_{exp}(\mu_\varepsilon)$	Num Peak load Strain ε_{num} (μ_ε)	ε_{exp}/ ε_{num}
			P_{exp} (kN)	P_{Num} (kN)				
1	S20-50x3-B	21.5	364	362	1.0055	10000	10300	0.969
2	S20-100x5-A	21.5	1352	1268	1.0662	9800	9500	1.018
3	S30-100x3-A	34.9	765	770	0.9935	4630	4900	1.017
4	S30-150x3-B	34.9	1209	1212	0.9975	3700	4000	0.925
5	SHS1C40	46.6	2768	2681	1.0325	10000	10000	1.000
6	SHS-5-C60	53	1488	1397	1.0651	7700	8300	0.928
7	S30-100x5B	34.9	1461	1323	1.1043	6893	7351	0.937
8	S30-150x1.6A	30	890	862	1.0325	6538	7149	0.914

Comparison of axial load (N) versus axial strain (ε) curves for different types of CFSST columns of experimental and numerical data obtained from Tao et al. also to compare with the self-numerical analysis with the same geometrical and mechanical data used by Tao. For each section three curve has been plotted with the data obtained from Tao experimental analysis in Figure 5.2.

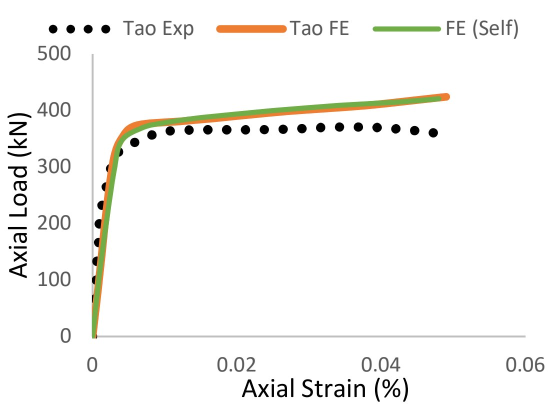

(a)

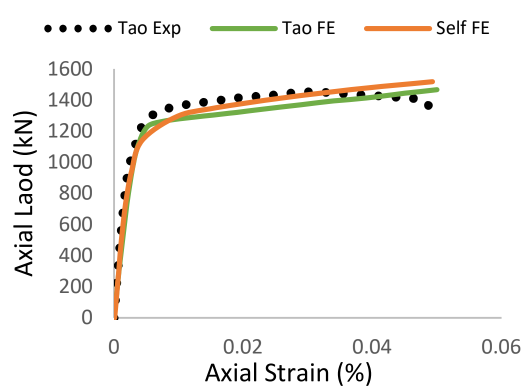

(b)

Figure 5.2 Tao et al. experimental and numerical behaviour of column groups, axial load vs deformation, (a) S20-50x3-B (51x2.85x150); (b) S20-100x5-A (101x5.05x300);

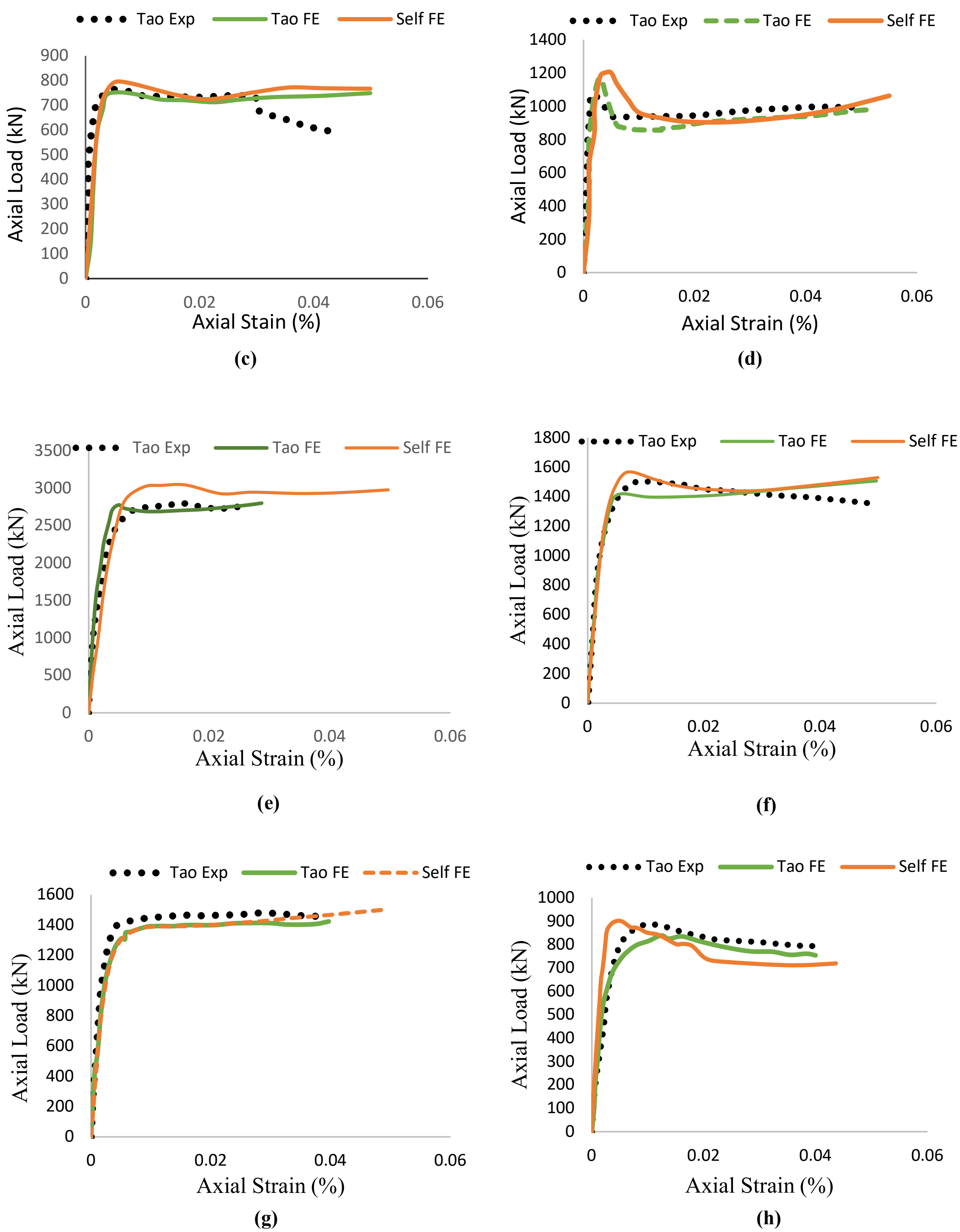

Figure 5.2 Tao et al. experimental and numerical behaviour of column groups, axial load vs deformation, (c) S30-100x3-A (100x2.85x300); (d) S30-150x3-B (152x2.85x450). (e) SHS-1C40 (100x2x300); (f) SHS-5-C60 (100x4.9x300); (g) S30-100x5B (101x5.05x300); (h) C30-150x1.6B (152.4x1.6x450)

Numerical investigation data was compared with Tao et al experimental data in Table 5.4 which presents the maximum axial compressive load and corresponding strain of the experimental tests. The ratio of the numerical to experimental capacities, P_{exp} /P_{num} ranges from 0.914 to 1.08 and corresponding standard deviation 0.002 which indicates the excellent performance of FE model in predicting the ultimate capacity of these FEC columns with the accuracy of 0.998 for concentrically loaded conditions. Again, the ratio of the numerical to Tao et al. experimental average axial strain at peak load, ε_{num} /ε_{exp} ranges from 0.914 to 1.18 and the corresponding standard deviations 0.0016 which indicate the accuracy of 0.998. In graphical representation it was observed that the experimental and FE curves almost merges with the each other so from the graphical points of view it is also indicate that experimental and numerical evaluation are very close in nature. Thereby it is obvious that the FE model analysis could predict the ultimate capacity and peak strain of CFSST columns with good accuracy.

5.5. Failure Modes

The failure modes of CFSST columns were identified from FE analysis compared with the failure modes observed in the current experiment. Failure modes were captured manually for all the specimens during the test. It was observed that, the failure pattern varied mostly due to change in cross section and slightly for change in concrete strength. The failure was at the corner due to bulging out of concrete in rectangular CFSST columns and in case of circular sections, the main failure was buckling failure, also it is observed that concrete crushing occurred before yielding of the stainless-steel plate. Similar failure behavior was obtained in the nonlinear FE simulation of CFSST columns under axial loads. The common failure pattern is shown in Figure 5.3.

Square CFSST Column

Circular CFSST Column

Figure 5.3: Experimental failure pattern

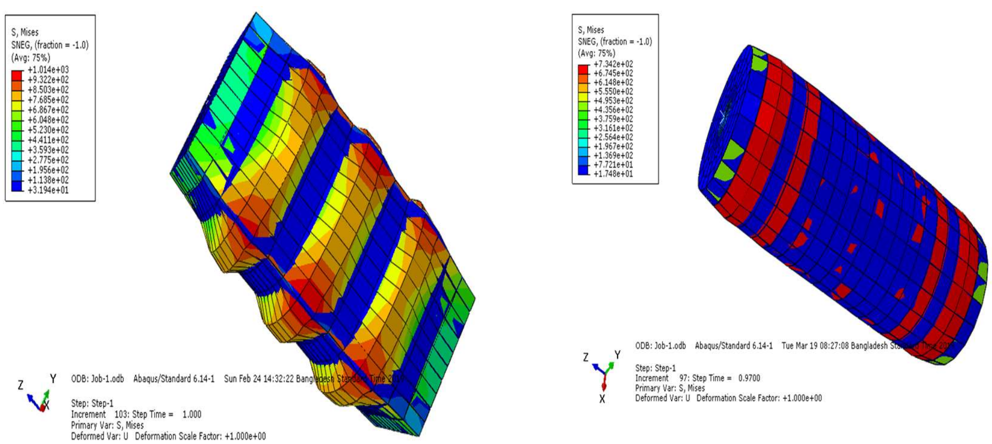

Square CFSST Column

Circular CFSST Column

Figure 5.4: Numerical failure pattern

5.6 Conclusions

Experimental analysis on behaviour of six sizes (3xsquare, 2xrectangular and 1xcircular) short CFSST columns subjected to short term axial load has been presented in this paper for three different concrete strengths (30, 40 and 50 MPa). The complete experimental load-deflection behavior of the composite column specimens has been attained in the study. This study also conducted a nonlinear 3D FE analysis on the current experimental test specimens' columns under axial load. The inelastic material properties of stainless steel and concrete have been incorporated in the models. Nonlinear material behaviour for concrete has been simulated in FE analysis. Geometric nonlinearities are also included in the model. The composite column strengths, axial shorting at failure and failure modes of the columns were predicted using FE model. The comparison between the experimental and numerical results showed that the FE models predict the experimental behaviour of CFSST columns under concentric gravity loads with the accuracy of 0.996 for peak load and 0.998 for stain at peak load.